Time-Optimal Trajectory Generation for 5-Axis On-the-Fly Laser Drilling

by

Ammar Alzaydi

A thesis

presented to the University of Waterloo

in fulfillment of the

thesis requirement for the degree of

Master of Applied Science

in

Mechanical Engineering

Waterloo, Ontario, Canada, 2011

AUTHOR'S DECLARATION

I hereby declare that I am the sole author of this thesis. This is a true copy of the thesis, including any required final revisions, as accepted by my examiners.

I understand that my thesis may be made electronically available to the public.

Ammar Ayad Alzaydi

Abstract

On-the-fly laser drilling provides a highly productive method for producing hole clusters (pre-defined groups of holes to be laser drilled) on freeform surfaced parts, such as gas turbine combustion chambers. Although the process is capable of achieving high throughputs, current machine tool controllers are not equipped with appropriate trajectory functions that can take full advantage of the achievable laser drilling speeds. While the problem of contour following has received previous attention in time-optimal trajectory generation literature, on-the-fly laser drilling presents different technological requirements, needing a different kind of trajectory optimization solution, which has not been studied prior to this thesis.

The duration between consecutive hole locations, which corresponds to the laser pulsing period, has to be kept constant, ideally throughout the part program. However, the toolpath between the holes is not fixed and can be optimized to enable the shortest possible segment duration. To preserve the dynamic beam positioning accuracy and avoid inducing excessive vibrations on the laser optics, the axis velocity, acceleration, and jerk profiles need to be limited. Furthermore, to ensure that hole elongation does not violate the given part tolerances, the orthogonal component of part velocity relative to the laser beam needs to be capped. All of these requirements have been fulfilled in the trajectory optimization algorithm developed in this thesis.

The hole locations are provided as pre-programmed sequences by the Computer Aided Design/Manufacturing software (CAD/CAM). A time-optimized trajectory for each sequence is planned through a series of time-scaling and unconstrained optimization operations, which guarantees a feasible solution. The initial guess for this algorithm is obtained by minimizing the integral square of the fourth time derivative (i.e. ‘snap’). The optimized trajectories for each cluster are then joined together or looped onto themselves (for repeated laser shots) using a time-optimized looping/stitching (optimized/smooth toolpath to repeat/loop a cluster or connect/stitch between consecutive clusters) algorithm. This algorithm also minimizes the integral square of jerk in the faster axes. The effectiveness of the overall solution has been demonstrated in simulations and preliminary experimental results for on-the-fly laser drilling of a hole pattern for a gas turbine combustion chamber panel. It is shown that the developed algorithm improves the cycle time for a single pass by at least 6% (from kinematic analysis

of the motion duration), and more importantly reduces the integral square of jerk by 56%, which would enable the process speed to be pushed up further.

Acknowledgements

This research is supported by Pratt and Whitney Canada, Ontario Ministry of Research and Innovation granting agencies in Canada and AUTO21.

I gratefully acknowledge the assistance of Dr. Amr Elfizy and Dr. Serafettin Engin and their feedback in the technical and experimental development in this thesis.

Valuable feedback on the scientific content and presentation of this thesis has been provided by Prof. J. Huissoon, and Prof. D. Wang. I would like to thank them for taking the time to read this thesis in its entirety.

I sincerely acknowledge the time and commitment that has been provided by my supervisor Prof. Kaan Erkorkmaz. His devotion to research and the success of his students is seen in everything he does. There are few words that can fully express my gratitude for his guidance and the experience he has provided over these past years. He has been a guide, mentor, teacher, and supporter.

Lastly, I thank my family for supporting, encouraging, and motivating me during my studies.

Dedication

I dedicate this thesis to my family who have always supported and encouraged me to achieve all of my ambitions and aspirations in life.

Table of Contents

List of Figures

List of Tables

Chapter 1

Introduction

1.1 Laser Drilling Overview

Manufacturers of turbine engines for aircraft propulsion and for power generation have benefited from the productivity of lasers for drilling small (0.3–1 mm diameter) cylindrical holes at 15-90º to the surface in cast, sheet metal and machined components. Their ability to drill holes at shallow angles to the surface at high rates per second has enabled new designs incorporating film-cooling holes for improved fuel efficiency, reduced noise, and lower Nitric Acid (NO), Nitrogen Dioxide (NO2) and CO emissions.

Incremental improvements in laser process and control technologies have led to substantial increases in the number of cooling holes used in turbine engines. Fundamental to these improvements and increased use of laser drilled holes is an understanding of the relationship between process parameters and hole quality and drilling speed.

Laser drilling is a successful manufacturing solution for many industries due to its advantages over conventional drilling techniques. Advantages include non-contact processing, low heat input into the material, flexibility to drill a wide range of materials, accuracy and consistency. Other benefits include drilling sub-micron holes and small holes with large aspect ratios and drilling at angles.

The common techniques used in drilling are percussion hole drilling, on-the-fly drilling and trepanning. Percussion drilling is a process where multiple pulses are applied per hole to achieve the desired results. High speed on-the-fly drilling is a percussion type drilling process where the holes are drilled with a single shot (or multiple shots at multiple passes) per hole while machine axes are moving, if multiple shots are needed per hole, then multiple passes are considered during on-the-fly drilling. Trepanning is a process by cutting large holes or contouring shaped holes.

Lasers can be focused to spot sizes as small as 10 – 20 microns. The high peak power coupled with short pulse widths, a perfect beam offers very good drilling capabilities in thin sheets, ceramics and silicon. The optics configuration is changed to achieve a different spot

size, required for drilling various hole diameters. High power lasers are also currently used for rock drilling applications, drilling of flow filters and strainers, sub-micron drilling in flexography ceramic rolls, high speed drilling of guide vanes, hole drilling of silicon, drilling diamonds for removing imperfections and on-the-fly drilling of cooling holes. The high peak and energy/pulse are also used for drilling thick metals.

This thesis focuses on laser drilling of cylindrical holes in turbine engine components, which generally occurs through melting and vaporization (also referred to as 'ablation') of the workpiece material through absorption of energy from a focused laser beam.

Manufacturers are applying results of process modeling and experimental methods to better understand and control the laser drilling process. The result is higher quality and more productive processes that in turn lead to better end products such as more fuel efficient and cleaner aircraft and power generating turbine engines.

1.2 Introduction

On-the-fly laser drilling provides a highly productive method for producing hole clusters on freeform surfaced parts, such as gas turbine combustion chambers [1]. Although the process is capable of achieving high throughputs, current machine tool controllers are not equipped with the appropriate trajectory functions that can take full advantage of the achievable laser drilling speeds. This thesis presents a new and time-optimized trajectory generation algorithm which addresses this problem.

Time-optimized trajectory generation has previously received attention in robotics and machine tool literature for contour following applications [2, 3, 4, 5]. There have also been successful works for following way-point data by modulating the time intervals in between the points [6]. However, the nature of on-the-fly laser drilling requires the motion duration between consecutive holes, which corresponds to the laser firing period, to be kept constant and minimized. In between the holes, the motion path is not fixed and can be modulated to achieve the maximum possible time reduction. This presents a new type of trajectory optimization problem, specific to on-the-fly laser drilling, which is studied for the first time in this thesis.

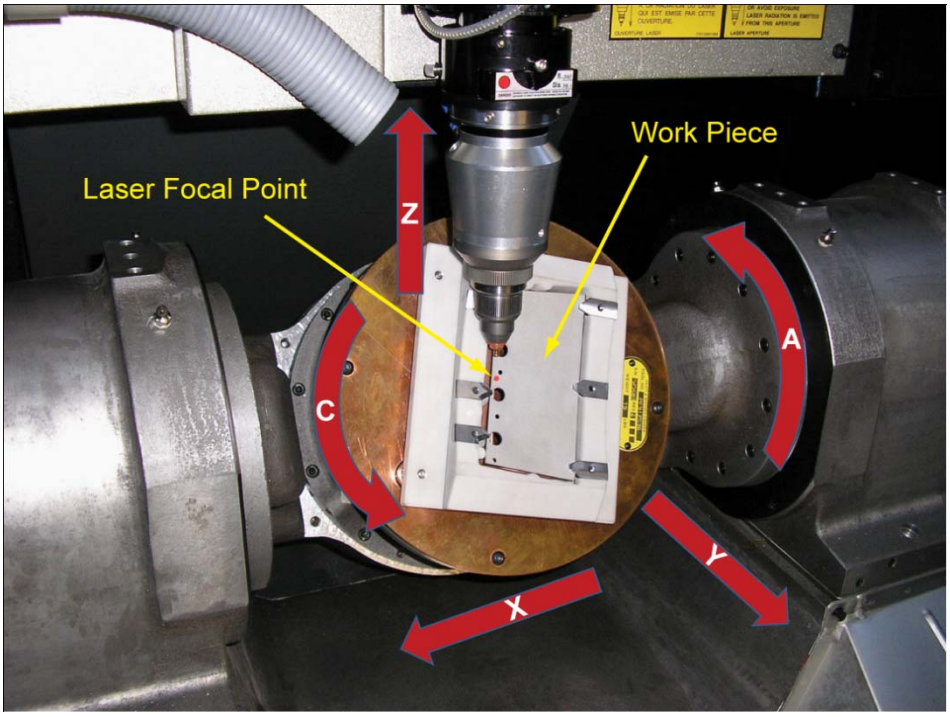

Figure 1.1: Configuration of 5-Axis Laser Drilling Machine Tool

Figure 1.1 shows a 5-axis laser drilling setup actuated by direct drive motors. Linear motors are used for motion in the x-, y-, and z-axes directions, and the trunion has a formation with two rotary axes (for rotary motions in the a- and c-axes). This machine was built for drilling gas turbine combustion chamber panel hole patterns like the one shown in Figure 1.2. Figure 1.2 also shows the numbered collections or groups of holes (clusters) that need to be drilled, in this specific example; there are 12 different clusters to be drilled by means of an optimized smooth trajectory. It is obvious that on-the-fly drilling of such a pattern requires full coordination of all 5-axes. The hole clusters are determined in the Computer Aided Design and Manufacturing software and each cluster needs to be drilled at a fixed laser pulsing frequency. After drilling a single cluster the connection between the clusters also has to be seamless with continuous smooth motion instead of decelerating and stopping at end of one cluster, repositioning at the beginning of the next cluster and accelerating at start of the drilling process for the consecutive clusters. The seamless cluster connection is performed in order to avoid unwanted vibrations on the machine and laser optics induced by aggressive and repetitive stopping and starting motions during the process. Hence, minimizing the duration of both cluster drilling and repositioning, while respecting

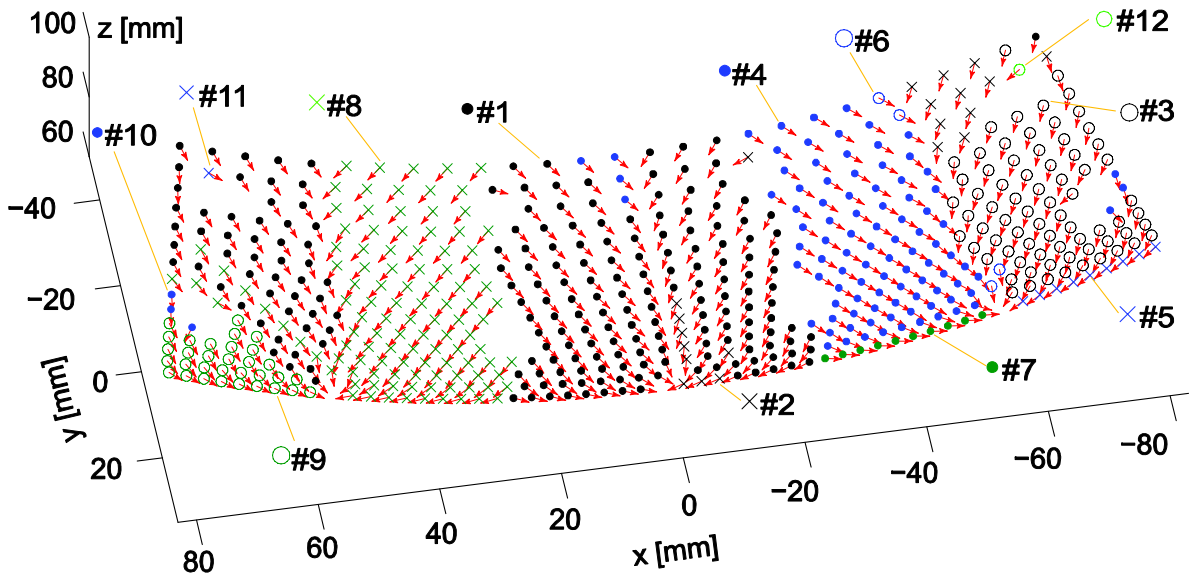

Figure 1.2: Hole Clusters and Orientations for a Turbine Combustion Chamber Panel

the physical limitations of the machine and process, is key to achieving high productivity in this operation. Currently, there exists no commercial interpolator or published technique prior to this study, which generates time-optimized trajectories for on-the-fly laser drilling.

The remainder of this chapter presents a brief cycle time analysis related to on-the-fly laser drilling, followed by an outline of the remaining chapters in this thesis.

1.3 On-the-Fly Laser Drilling Vs. Percussion Drilling

During the process of drilling a turbine engine panel, on-the-fly laser drilling is highly desirable over percussion drilling. During on-the-fly drilling, the laser beam fires a single pulse at the hole location, removing a limited amount of material from the panel, and moves to fire at a different location (consecutive holes in a cluster). This allows the previous hole locations which already experiences a single laser shot to cool down before it experiences a second and third laser drilling shots. This produces cleaner drilled holes. In percussion drilling the laser optics are positioned at the hole location and all desired number of shots are fired to fully drill the hole before moving to drill the consecutive holes. This melting and vaporization (Ablation) of material is considered to be a less cleaner process than on-the-fly drilling, as material overheating might occur, deforming the hole shapes, and if a cool down

time is allowed between percussion laser shots, this will end up increasing the overall drilling cycle time significantly.

1.4 Feasibility of On-the-Fly Laser Drilling

On-the-fly laser drilling may not always be the most productive solution, especially when precision drilling requires each hole to be drilled with multiple laser shots. In this case, percussion drilling (i.e., coming to a full stop at each hole and firing a sequence of shots) may be a more productive solution. In percussion drilling, the drilling frequency can also be increased to speed up the process. However, a drop in the laser power, due to higher pulsing frequency, can also be expected. In practice this is compensated by firing more shots per hole.

The following analysis investigates the time efficiency of both methods and shows the condition for which on-the-fly drilling produces a shorter cycle time:

N : Number of holes in a single cluster

n_{Fly} : Number of shots per hole for on-the-fly drilling

n_{Per} : Number of shots per hole for percussion drilling

T_{Fly} : Average segment travel duration for on-the-fly drilling

T_{Per} : Average duration for hole repositioning in percussion drilling

T_L : Laser firing period in percussion drilling (while axes are at rest)

D_{Fly} : Total process duration when on-the-fly drilling is used

D_{Per} : Total process duration when percussion drilling is used

The total duration required for each operation can be expressed as:

$$D_{Fly} = N\ n_{Fly} T_{Fly} \tag{1.1}$$

$$D_{Per} = N T_{Per} + N\ n_{Per} T_L \tag{1.2}$$

For on-the-fly drilling to be more time efficient than percussion drilling, Eq. (1.3) must hold:

$$D_{Fly} < D_{Per} \tag{1.3}$$

Substituting Eqs. (1.1) and (1.2) into (1.3):

$$N\ n_{Fly} T_{Fly} < N T_{Per} + N\ n_{Per} T_L$$

Resulting in:

$$T_{Fly} < \frac{T_{Per}}{n_{Fly}} + \frac{n_{Per}}{n_{Fly}} T_L \tag{1.4}$$

Considering a simple example where $n_{Fly} = n_{Per}$ (i.e., no power drop due to higher frequency laser pulsing) and $T_{Fly} = T_{Per} = T_L$ (i.e., the machine tool's feed drives are fast enough to re-position the holes at the pulsing rate of the laser), it can be verified that:

$$T_{Fly} < (1 + \frac{1}{n_{Fly}}) T_{Per} \tag{1.5}$$

For a case involving 8 laser shots per hole, it can be verified that on-the-fly drilling will be at least 11% faster than percussion drilling. For 2 shots per hole, the speed increase becomes 33%.

However, in practical cases, the laser frequency is faster than the hole repositioning speed of the feed drives, which is the main motivation behind developing a time-optimized trajectory generation algorithm for on-the-fly laser drilling. Such an algorithm should ideally satisfy the condition in Eq. (1.4), which makes on-the-fly laser drilling more time-efficient than the alternative method of percussion drilling.

In addition to cycle time, the vibration delivered to the machine structure, particularly the laser optics, also plays a vital role in determining the productivity of a laser drilling operation. Excessive vibrations can cause the optics to lose alignment quickly, thereby requiring extensive downtime for realignment. Rather than stopping at each hole, as is the case in percussion drilling, the continuous motion employed by on-the-fly drilling can dramatically reduce the high frequency content in the acceleration profiles, by reducing the jerkiness of the motion commands. This in turn can lead to a significant improvement in the overall productivity of the process. Hence, kinematic cycle time alone cannot be used as the sole deciding factor in choosing between on-the-fly and percussion drilling. The impact of the process parameters and trajectory used in each operation, on the overall productivity, cost-effectiveness, and part quality also needs to be considered.

1.5 Thesis Outline

In the remainder of this thesis, Chapter 2 presents a literature review of the state-of-the-art in machine tool trajectory planning. Chapter 3 provides an overview of the optimization

problem and proposed solution. Chapter 4 presents details of hole cluster trajectory optimization. Chapter 5 presents a method to seamlessly stitch pre-optimized cluster trajectories in minimal time and with minimal jerk. Implementation results validating the effectiveness of the proposed algorithm are presented in Chapter 6. The conclusions of this thesis and future research steps are described in Chapter 7. Appendices A through C are provided to explain in detail and prove some of the mathematical derivations used in this thesis.

Chapter 2

Literature Review

2.1 Introduction

This chapter presents a review of literature and industrial state-of-the-art in the area of trajectory planning for robots and in particular, machine tools. In Computer Numerical Control (CNC) of machine tools, the toolpath geometry and progression along the geometry (i.e. feedrate) are typically planned as separate tasks, similar to the schematic in Figure 2.1.

Figure 2.1 shows that computationally intensive tasks such as the toolpath parameterization and integration of the segment arc-length are generally handled by the CAM system in an offline environment, whereas feed generation and trajectory interpolation are realized in the CNC controller in real-time. Feedrate generation and optimization are interfaced subtasks of the trajectory generation module in the CNC controller.

Nevertheless, they both influence the smoothness of the final interpolated trajectory. Considering that a point along a path defined in Cartesian space can be represented in vector form: $\boldsymbol{r} = \boldsymbol{r}(s) = [x(s)\ y(s)\ \mathrm{z(s)}]^T$ as a function of the path parameter s, coming up with the definition of $\boldsymbol{r} = \boldsymbol{r}(s)$ constitutes the path planning task, and determining the progression along the path as a function of time (i.e., $s = s(t)$) is the feedrate planning task. The velocity, acceleration, and jerk profiles can be determined by applying the chain rule as follows:

$$\begin{aligned} \dot{\boldsymbol{r}} &= \boldsymbol{r}_s \dot{s} \\ \ddot{\boldsymbol{r}} &= \boldsymbol{r}_{ss} \dot{s}^2 + \boldsymbol{r}_s \ddot{s} \\ \dddot{\boldsymbol{r}} &= \boldsymbol{r}_{sss} \dot{s}^3 + 3\boldsymbol{r}_{ss} \dot{s}\ddot{s} + \boldsymbol{r}_s \dddot{s} \end{aligned} \tag{2.1}$$

Above, $\boldsymbol{r}_s = d\boldsymbol{r}/ds$, $\boldsymbol{r}_{ss} = d^2\boldsymbol{r}/ds^2$, $\boldsymbol{r}_{sss} = d^3\boldsymbol{r}/ds^3$, $\dot{s} = ds/dt$, $\ddot{s} = d^2s/dt^2$, $\dddot{s} = d^3s/dt^3$. It is clear that in order to get a smooth trajectory with continuous profiles up to acceleration level, and bounded profiles up to jerk level, the corresponding geometric ($\boldsymbol{r}_s$, $\boldsymbol{r}_{ss}$, $\boldsymbol{r}_{sss}$) and time derivatives ($\dot{s}, \ddot{s}, \dddot{s}$) also need to satisfy similar conditions for continuity and boundedness. This has motivated extensive research in trajectory generation methods in

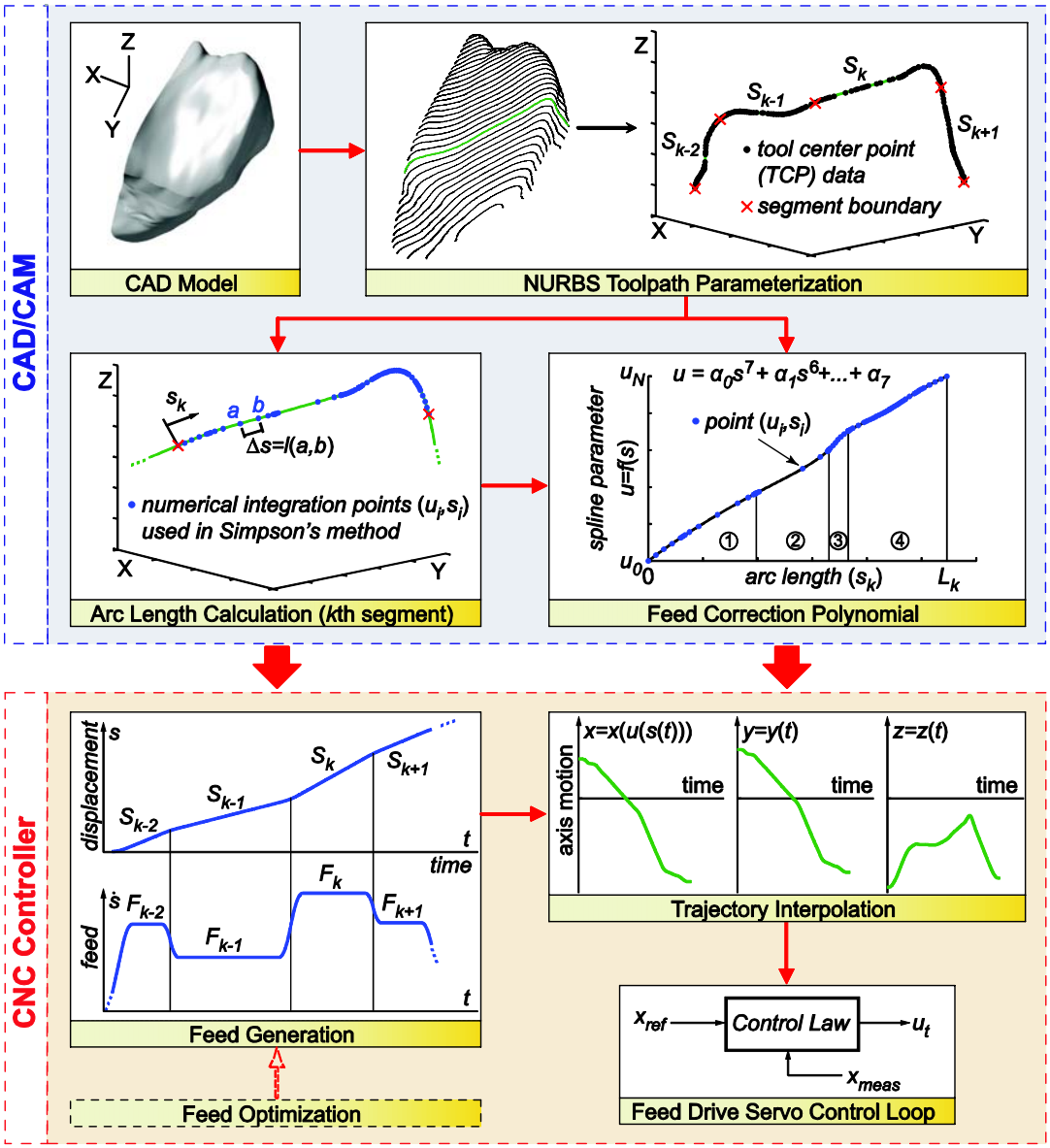

Figure 2.1: Overview of Trajectory Generation in Machine Tools (From Heng [7])

terms of toolpath planning, interpolation, and feedrate generation, as will be explained in Sections 2.2 and 2.3.

When allowable, modulating the feedrate to achieve the shortest possible cycle time contributes to the productivity of the manufacturing operation being carried out. However, except for very simplistic cases, where only velocity and acceleration limits are considered, coming up with a time-optimal feed profile which limits the axis jerk values is a non-trivial task. The work conducted in this area has also been summarized in Section 2.3.

Compared to traditional machining operations, where the toolpath has to follow a continuous contour, on-the-fly laser drilling poses significantly different technological requirements. To the best of the author's knowledge, trajectory optimization for on-the-fly laser drilling has not received extensive investigation prior to this thesis. On-the-fly laser drilling requires the travel duration between consecutive hole locations, which corresponds to the laser firing period, to be kept constant and minimized throughout the part program. The toolpaths between the holes, however, are not restricted in shape and can be modulated to allow the maximum possible reduction in the laser firing period. Since the drilling is realized while the part is in relative motion with respect to the beam, hole elongation needs to be considered and capped in order to avoid violating the part tolerances. The hole elongation constraint is explained in detail in Chapter 3. In addition, the machine tool's 5-axis kinematics and velocity, acceleration, and jerk limits also need to be taken into account. These issues have been considered and incorporated into the trajectory optimization algorithm developed in this thesis. A brief review of the existing work related to laser drilling is presented in Section 2.4. The chapter ends with a summary in Section 2.5.

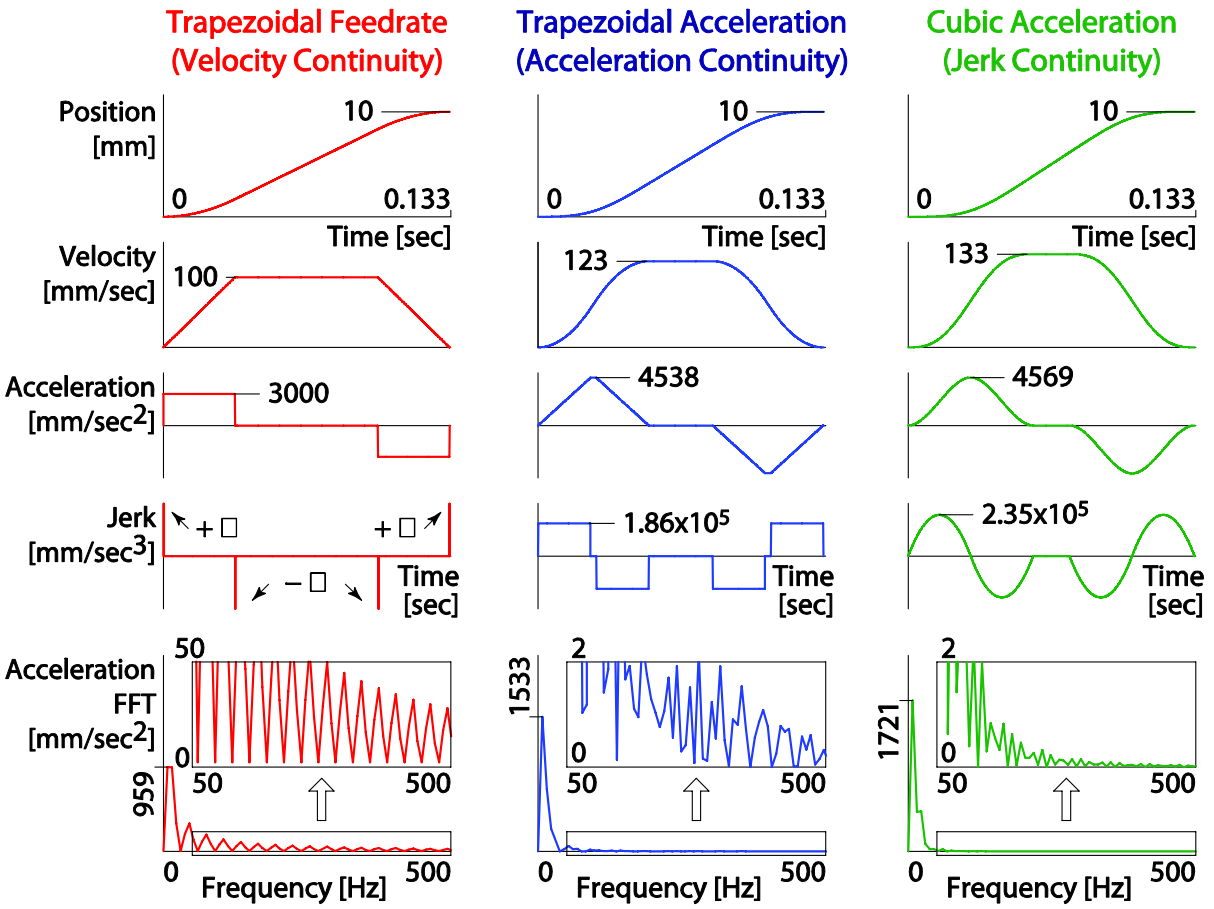

Figure 2.2: Time and Frequency Domain Comparison of 3 Different Trajectory Types

2.2 Toolpath Planning and Interpolation

It is well-known that discontinuities in the position commands can lead to large spikes in the velocity, acceleration, and jerk profiles. This, in turn, results in undesirable high-frequency harmonics in the motor force or torque, which can excite the natural modes of the mechanical structure or servo control system. Figure 2.2 provides a comparison between velocity-, acceleration-, and jerk-continuous motion. As the motion becomes smoother, the high frequency content in the acceleration harmonics diminishes dramatically, thus reducing the high frequency excitation delivered to the machine tool structure.

High-frequency harmonics can also cause actuator saturations (by pushing the actuators beyond their functional limits) or axis tracking errors as a result of actuator saturation, meaning that the axes are incapable of following the reference position commands, thus causing deviations from desired trajectory, thereby resulting in violations of the part

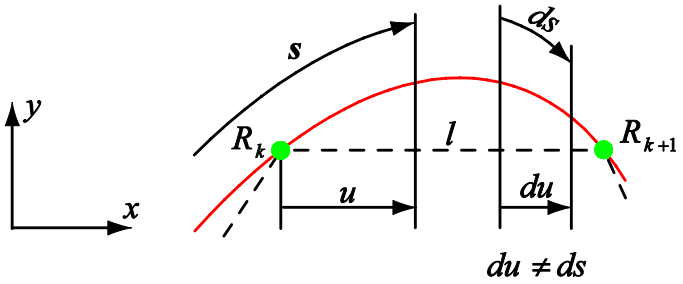

s : *Arc Displacement*
u : *Spline Parameter – Along Chord Between Two Points*
l : *Chord Length*
k : *Segment Number*

Figure 2.3: Parameter (u) and Actual Path (s) Increments in Spline Interpolation

manufacturing tolerances. Considering this effect, employing only linear and circular interpolation techniques to machine complex shapes such as dies, molds, turbine blades, and aerospace parts has serious limitations in term of productivity, since the machine tool must decelerate/accelerate or stop between consecutive G codes [8, 9]. Therefore, a great deal of work has been done to overcome these problems by developing spline toolpath definitions for three [7, 10-22] and five axis machine tools [23-27], which yields paths with second order or higher levels of continuity.

One of the main issues with spline toolpath planning is that the curve parameter (shown with u in Figure 2.3) is not necessarily equal to the spline arc length (shown with s in Figure 2.3). Since, in general $ds/du \neq 1$, the values of the spline parameter have to be carefully computed for each desired arc increment, in order to avoid inducing unwanted speed fluctuations. As measures to solve this problem, researchers have tried to either parameterize the spline toolpath to keep the value of ds/du as close to one as possible [12, 13, 14], or they have devised Taylor series, feed correction polynomial-based, or iterative interpolation methods, which minimize unwanted feed fluctuations while interpolating the spline toolpaths [7, 9, 11, 14, 19, 28-35].

During on-the-fly laser drilling, since the toolpath is not fixed between the hole locations, maintaining constant feed is less of an issue, but coming up with an appropriate toolpath that will allow the highest travel speed while keeping the relevant kinematic profiles within the machine's and process' limits is crucial.

2.3 Feed Motion Generation & Optimization

In feed generation, it is essential to have continuous acceleration profiles, and bounded jerk, in order to avoid generating unwanted high frequency content in the motion commands. In this respect, various jerk bounded [11, 36, 37, 38] and jerk continuous [19, 39-43] feed generation techniques have been proposed in literature. In addition, when the manufacturing process allows, optimizing the feed profile to minimize the cycle time can result in significant cost savings and productivity increase. Some of the feed optimization work has been pioneered in the robotics and machine tool literature with [2] and [44, 45], which at initial stages resulted in acceleration discontinuous trajectories that were fast, but detrimental to the production machinery. Later, as jerk and torque rate limits and cutting process model were considered, various feed optimization methods have emerged which are highly effective [3-6, 19, 46- 54]. Some of these methods make some kind of optimality trade-off in favour of faster computational speed, which are often in the form of constraining the feed profile to well-known shapes for easy mathematical solution, or adopting conservative feed limits based on worst-case assessments. On the other hand, elaborate techniques like the one in [3], which utilizes full-blown sequential quadratic programming [55], yield the shortest cycle times. However, such complicated methods are still not practical for on-line implementation. Ideally, the solution sought in this thesis for on-the-fly laser drilling should be both easy and simple to implement, and also converge closely to a globally optimal solution (with minimal restriction on the trajectory profile shapes). Although off-line implementation is targeted, excessive processing times are not acceptable.

There have also been studies to generate quick and smooth axis trajectories by minimizing the integral square of jerk [56-60], which has its roots in characterizing the movement of humans and primates [61]. In this thesis, this idea has been taken one level further, by investigating the outcome of minimizing the integral square of the fourth time derivative (i.e. ‘snap’), which has been found to yield an initial guess that is very close to the desired time-optimal trajectory for on-the-fly laser drilling.

2.4 Literature on Laser Drilling

Laser drilling provides a highly productive method for producing hole clusters on freeform surfaced parts. While there have been detailed studies that characterize the process of laser drilling [62, 63] and evaluate various machine configurations [1], only a limited amount of prior work has been done related to trajectory planning in this area [64, 65, 66]. To the best of the author's knowledge, trajectory optimization for on-the-fly drilling has not even been studied prior to this thesis.

While the algorithm in [65] considers the optimal sequencing of hole locations based on travel distance, the trajectory generation technique in this thesis assumes that the holes are already sequenced by the Computer Aided Design/Manufacturing (CAD/CAM) software, and solves the time-optimal solution for traversing these holes on-the-fly. [66] solves a general time-optimal trajectory problem in the presence of obstacles, but does not take into account the process constraints related to on-the-fly laser drilling, such as the fixed laser pulsing frequency, or the hole elongation problem. It deals with the problem of determining the optimum route for an end effector that visits a number of task points in a similar but not identical fashion to the well-known travelling salesman problem (TSP). The authors suggest that the measure to be optimized is time instead of distance, and the travel time between two points is significantly affected by the manipulator configuration. Therefore, solutions of the inverse kinematics problem need to be taken into consideration. [67] provides process models and trajectory planning techniques for preserving sharp cornered geometries during laser cutting.

This thesis presents the time-optimized trajectory solution for the case where clusters of holes are pre-sequenced, and they need to be drilled at a constant laser pulsing frequency. In order to ensure that hole elongation does not cause tolerance violations, the 5-axis kinematics of the machine tool are also considered [68, 69, 70]. Axis level velocity, acceleration, and jerk limits are considered throughout the part program. Rather than following the traditional method used in machine tool trajectory planning, by planning the toolpath and feed profile separately, the kinematic profile for each axis is directly formulated as a function of time. This greatly simplifies the solution of the optimization problem.

Following the problem definition stated in Chapter 3, Cycle time optimized trajectories for each cluster are solved using the technique devised in Chapter 4. These trajectories are

stitched together, or looped back onto themselves (for repeated laser shots), using the algorithm in Chapter 5. The intermediate and final results obtained during this master's research have been published in [71] and [72]. Currently, the algorithm is being integrated at the industrial partner's premises, for use in the production of gas turbine combustion chambers.

2.5 Summary

This chapter has presented a survey of the academic literature and industrial practice relevant to multi-axis laser toolpath planning, feed generation for machine tools, and some of the issues specific to laser drilling. The challenges related to spline toolpath generation, interpolation, and feedrate optimization have been discussed. The proposed solution in this thesis differs from the traditional machine tool trajectory generation architecture, and lends itself to an easier mathematical formulation and solution by formulating all of the kinematic profiles directly as a function of time. Details of the proposed algorithm are discussed in the proceeding chapters.

Chapter 3

Optimization Problem and Proposed Solution Strategy

3.1 Problem Definition

Unlike a 3-axis system, 5-axis machining center has a non-Cartesian kinematic structure that, in some applications, requires transformation of the tool tip position and tool axis orientations programmed in the CAM systems into reference joint position commands using the inverse kinematics. In this thesis, 5-axis machine forward kinematics are used to translate hole locations from an NC file (where joint positions are given with respect to time) into part coordinates with respect to a laser focal point and with respect to the fixed drilled part. The machine inverse kinematics were not needed, as all joint positions at given instances in time are given for each hole location. In return, using 5-axis laser drilling allows the achievement of holes drilled at desired angles on a flat or curved surface for aerospace applications, which is the focus of this thesis.

The overall objective is to generate 5-axis acceleration-continuous trajectories that minimize the cycle time required to produce on-the-fly laser drilled parts subject to machine tool and process constraints. Defining the joint vector for the machine's translating (x, y, z) and rotating (a, c) axes:

$$\boldsymbol{q} = [x \quad y \quad z \quad a \quad c]^T \tag{3.1}$$

the machine constraints considered (in addition to each axis translational and rotational displacement limits) are that axis velocity ($\dot{\boldsymbol{q}}$), acceleration ($\ddot{\boldsymbol{q}}$), and jerk ($\dddot{\boldsymbol{q}}$) be kept within their limits. Velocity limits ($\boldsymbol{v}_{\max} = [\dot{x}_{\max} \quad \dots \quad \dot{c}_{\max}]^T$) are provided by the machine tool manufacturer in accordance with the stroke and acceleration capabilities and guide-way life characteristics. Acceleration limits ($\boldsymbol{a}_{\max} = [\ddot{x}_{\max} \quad \dots \quad \ddot{c}_{\max}]^T$), along with velocity limits, help indirectly limit the maximum force or torque requirement. This ensures that the drives operate within their linear range without saturation. Acceleration limits may also be replaced by force or torque limits, should a dynamic model of the machine be available along with experimentally identified inertia and damping values [2, 3]. Although this approach results in less conservative cycle times, full identification of a machine's dynamics may not always be

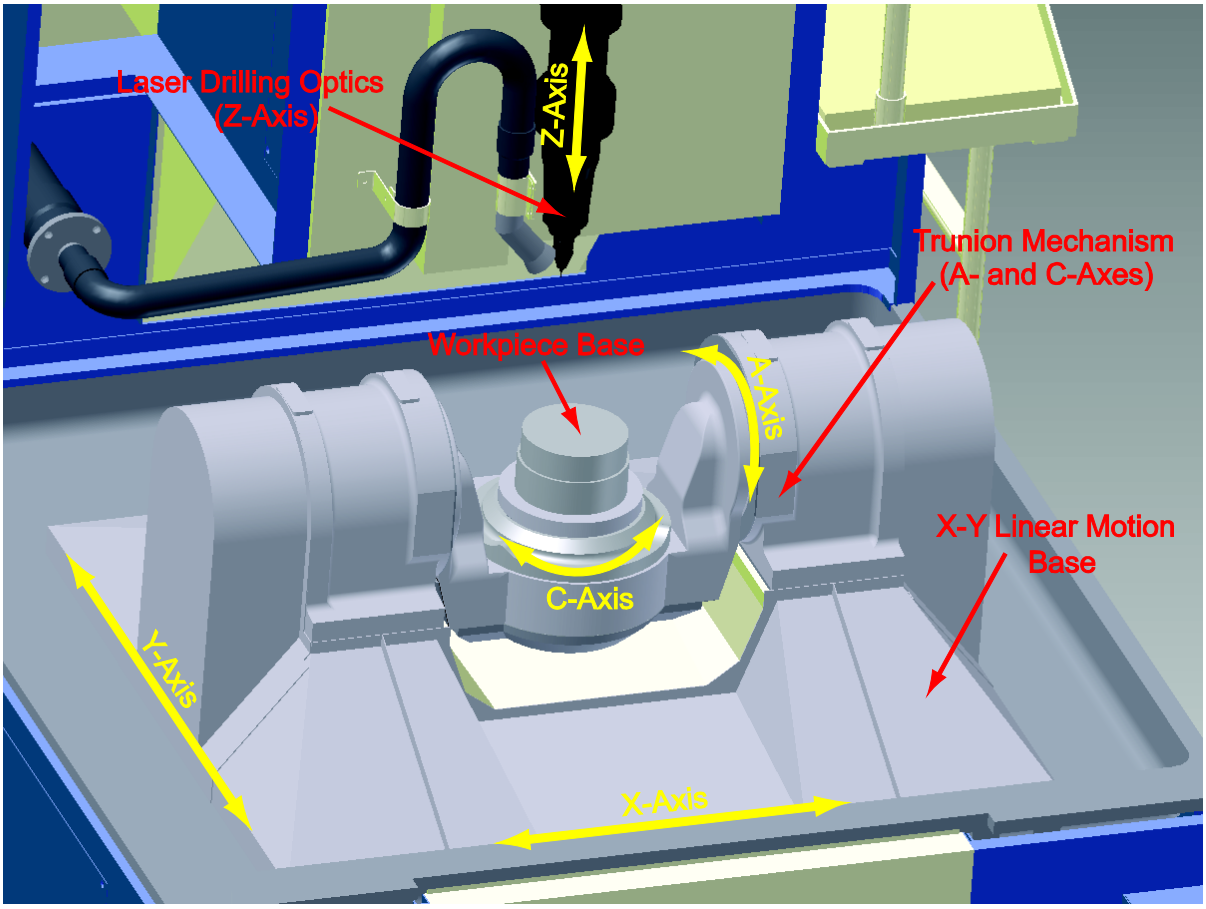

Figure 3.1: 3D Representation of 5-Axis Laser Drilling Machine

practical. In this case, acceleration limits readily provided by the manufacturer, or adopted by the end user, may be used as done in [5] and also in this work. Figure 3.1 shows a 3D model of the machine being used for this thesis.

The jerk limits ($\boldsymbol{j}_{\max} = [\dddot{x}_{\max} \quad \dots \quad \dddot{c}_{\max}]^T$) help constrain the high frequency content in the commanded motion, which indirectly limits the instantaneous value of tracking error. This helps retain the beam positioning accuracy during high traverse rates. Limiting jerk also reduces the amount of vibration induced on the machine structure, in particular the laser optics. Since excessive vibration causes the optical assembly to lose alignment after a relatively short production run, which requires extensive downtime for realignment, limiting the jerk also has a positive influence on the productivity of the laser drilling operation.

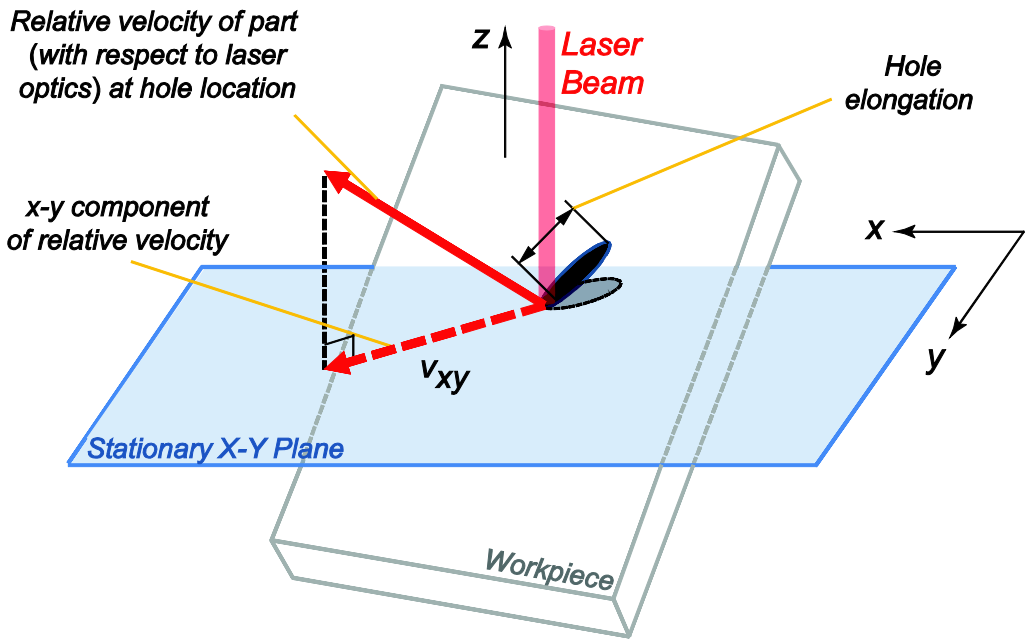

Figure 3.2: Hole Elongation Due to X-Y Component of Part Velocity

There is also a process constraint that needs consideration. The part is in relative motion with respect to the beam during drilling and this causes elongation of holes, as illustrated in Figure 3.2. If this velocity component exceeds a certain limit, then the hole elongation may violate the part tolerances. The laser is aligned with the z-axis of the machine. Hence, the x-y component of the workpiece velocity at the hole location (v_{xy}) relative to the laser optics needs to be limited. Considering the 5-axis configuration shown in Figure 1.1, and following the kinematic analysis presented in Appendix A, this velocity component can be computed as:

$$\left.\begin{aligned} v_{xy} &= \sqrt{v_x^2 + v_y^2} \quad \text{where:} \\ v_x &= \dot{x} - (x_h \sin c + y_h \cos c)\dot{c} \\ v_y &= \dot{y} + \left[(x_h \cos c - y_h \sin c)\cos a\right]\dot{c} \\ &\quad - \left[(x_h \sin c + y_h \cos c)\sin a + z_h \cos a\right]\dot{a} \end{aligned}\right\} \tag{3.2}$$

Above, (x_h, y_h, z_h) represents the hole location in the part coordinate system (C.S.4 in Appendix A). Using the knowledge that the laser focus (i.e., drilling) point is programmed to coincide with the origin (i.e., (0,0,0)) of the machine's coordinate system, the hole location (x_h, y_h, z_h) can be computed from commanded axis motion as:

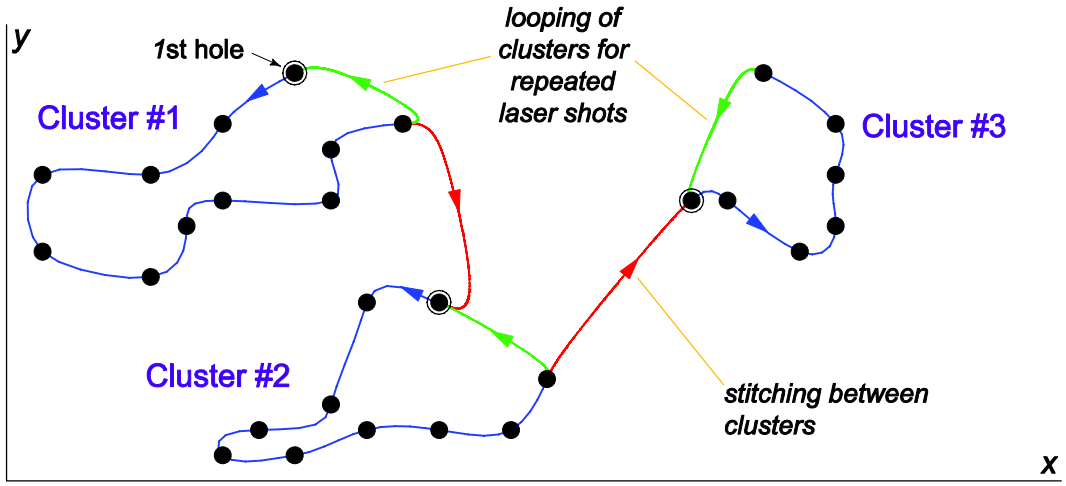

Figure 3.3: Overall Strategy Comprising of: 1) Optimizing Each Cluster Separately, 2) Looping/Stitching of Individual Clusters with Time-Optimal Segments.

$$\begin{bmatrix} x_h \\ y_h \\ z_h \end{bmatrix} = \begin{bmatrix} \cos c & \cos a \sin c & \sin a \sin c \\ -\sin c & \cos a \cos c & \sin a \cos c \\ 0 & -\sin a & \cos a \end{bmatrix} \begin{bmatrix} -x \\ -y \\ z \end{bmatrix} \tag{3.3}$$

derivation of Eq. (3.3) can also be found in Appendix A.

The process of trajectory generation in this thesis is open loop (without joint feedback from the machine controller) and assumes that the machine positioning controller is functioning properly at all times. Therefore, in Appendix A, only the forward kinematics is calculated. The inverse kinematics is handled inside the CAD/CAM system and the calculations of joint or axis values during operation are not necessary for this work.

While the machine related velocity, acceleration, and jerk constraints need to be respected at all times, the hole elongation constraint needs to hold only at the hole locations, thereby allowing higher x-y plane velocities to be reached in between the holes. This yields less conservative cycle time compared to enforcing this constraint throughout the motion.

Hence, the constraints can be formally stated as:

$$\left.\begin{array}{ll} \text{Velocity} & -\boldsymbol{v}_{\max} \le \dot{\boldsymbol{q}} \le \boldsymbol{v}_{\max} \\ \text{Acceleration:} & -\boldsymbol{a}_{\max} \le \ddot{\boldsymbol{q}} \le \boldsymbol{a}_{\max} \\ \text{Jerk:} & -\boldsymbol{j}_{\max} \le \dddot{\boldsymbol{q}} \le \boldsymbol{j}_{\max} \\ \text{Hole Elongation:} & -v_{xy,\max} \le v_{xy} \le v_{xy,\max} \end{array}\right\} \tag{3.4}$$

3.2 Overview of Proposed Solution

The solution developed in this trajectory optimization work comprises of two main steps, as illustrated in Figure 3.3:

Step #1: Find a time-optimized on-the-fly drilling trajectory for each cluster (pre-determined and defined group of holes to be laser drilled) which minimizes the laser pulsing period T :

$$\min T \tag{3.5}$$

Since the toolpath can be freely modulated between the holes, the objective in this step is to find the optimized path geometry that will enable the shortest possible traverse time between the consecutive holes inside a cluster. This trajectory must have at least acceleration level (C^2) continuity and it must also be bounded in jerk. A four sub-step technique has been developed in Chapter 4, as the solution to this problem.

Step #2: Determine time-optimized looping and stitching (optimized/smooth path to repeat/loop a cluster or connect/stitch between consecutive clusters) segments to allow seamless repetition and connection of clusters:

The idea of looping and stitching is to make a seamless connection with given position and velocity boundary conditions while finding the minimal motion cycle time. This is used for looping a cluster during multiple laser drilling passes, or making a connection between consecutive clusters in the part program. In this thesis, a procedure is presented that first solves the time-optimized trajectory for each axis, and then synchronizes the total motion duration among multiple axes by slowing down the faster axes to accommodate the slowest one(s). While doing so, the kinematic solutions for the faster axes are also optimized to minimize the integral square of jerk. The full details of the solution are presented in Chapter 5.

3.3 Conclusion

This chapter has provided the problem definition and an overview of the proposed solution for time-optimized laser drilling trajectory optimization. At this stage, the overall laser drilling trajectory cycle time optimization problem is divided into two main steps; 1. Time-optimized trajectory for laser drilled clusters. 2. Smooth and time-optimized stitching motion for repeated cluster drills or connection between consecutive clusters. Each step is optimized independently. Therefore, it is assumed that a best scenario in both steps will provide an overall time-optimized solution. In future work, an optimization function can consider different scenarios from both main steps to determine the appropriate optimal or sub-optimal combination of both steps that guarantees the global optimality of the combined solutions of both steps. The following chapters will detail the individual methods developed and results obtained in this thesis.

Chapter 4

Cluster Trajectory Optimization

4.1 Introduction

In cluster trajectory optimization (with pre-defined groups of holes that were clustered according to an existing algorithm in the CAD/CAM software), the quintic spline has been chosen as the basis curve due to its simplicity and sufficient degrees of freedom, enabling different C^2 parameterizations all passing through the same way-points (i.e., hole locations). Assuming there are $N+1$ holes in the cluster, and the travel duration between consecutive holes is equal to the laser firing period T, which is constant, the k^{th} segment describing the x-axis motion connecting holes k to k+1 can be expressed as:

$$[x(\tau)]_k = A_{xk}\tau^5 + B_{xk}\tau^4 + \ldots + F_{xk} \quad , \quad 0 \le \tau \le T \tag{4.1}$$

Figure 4.1: A Single Quintic Segment Parameterized By Its Boundary Conditions

The motion in the other axes can be parameterized similarly. Considering Figure 4.1, if position (X_k, X_{k+1}), velocity ($\dot{X}_k, \dot{X}_{k+1}$), and acceleration ($\ddot{X}_k, \ddot{X}_{k+1}$) boundary conditions at the hole locations are known, then the spline coefficients can be uniquely determined through Eq. (4.2) [70], and vice-versa with Eq. (4.1).

$$\left.\begin{aligned} A_{xk} &= [6(X_{k+1} - X_k) - 3(\dot{X}_{k+1} + \dot{X}_k)T + 0.5(\ddot{X}_{k+1} - \ddot{X}_k)T^2]/T^5 \\ B_{xk} &= [15(X_k - X_{k+1}) + (7\dot{X}_{k+1} + 8\dot{X}_k)T + (1.5\ddot{X}_{k+1} - \ddot{X}_k)T^2]/T^4 \\ C_{xk} &= [10(X_{k+1} - X_k) - (4\dot{X}_{k+1} + 6\dot{X}_k)T - (1.5\ddot{X}_{k+1} - 0.5\ddot{X}_k)T^2]/T^3 \\ D_{xk} &= 0.5\ddot{X}_k, \qquad E_{xk} = \dot{X}_k, \qquad F_{xk} = X_k \end{aligned}\right\} \tag{4.2}$$

The optimized trajectory for a cluster is found by applying the four sub-steps in Figure 4.2, which are detailed in the following.

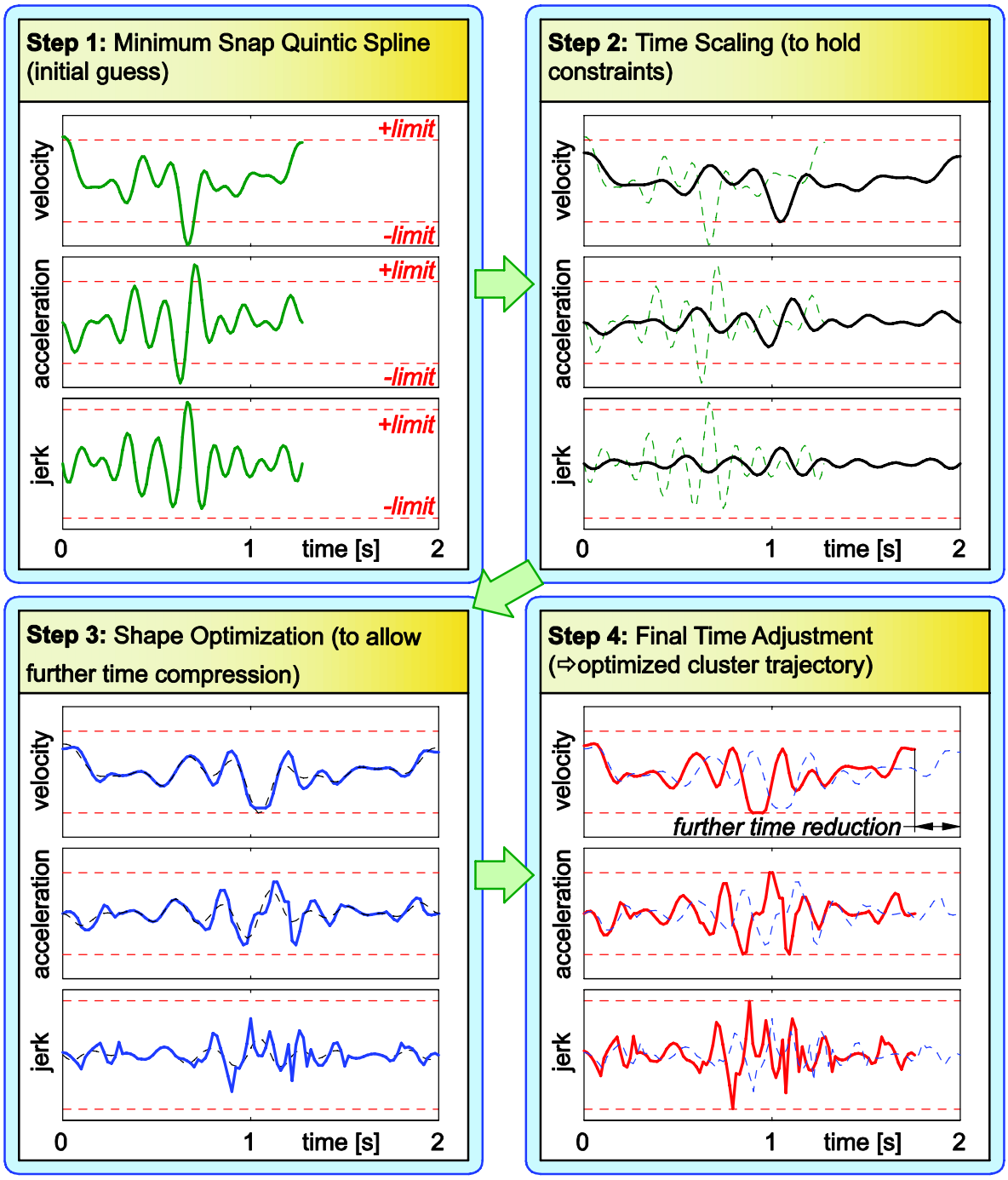

Figure 4.2: Overview of Cluster Trajectory Optimization.

4.2 Step 1: Minimum Snap Quintic Spline

First, a smooth trajectory is fit which traverses through the holes assuming a nominal segment duration T. This serves as an initial guess towards finding the final time-optimized solution. Through trials and using different objective functions for the shape optimization step (explained in Appendix B), it was found that minimizing the integral square of the fourth time derivative (i.e., 'snap') while enforcing jerk level continuity constraints resulted in an initial guess reasonably close to the final optimized solution. Therefore, this approach is adopted here. Considering that the parameters for a single segment can be grouped as $\boldsymbol{\theta}_{xk} = [A_{xk} \dots F_{xk}]^T$ ($k = 1, 2, \dots, N$), the overall parameter vector for a cluster of N segments becomes: $\boldsymbol{\theta}_x = [\boldsymbol{\theta}_{x1}^T \dots \boldsymbol{\theta}_{xN}^T]^T$. The minimum snap objective is expressed as:

$$\min_{\boldsymbol{\theta}_x} \int_0^{NT} [\frac{d^4 x}{dt^4}(t)]^2 dt = \min_{\boldsymbol{\theta}_x} \frac{1}{2} \boldsymbol{\theta}_x{}^T \mathbf{K} \boldsymbol{\theta}_x \tag{4.3}$$

For the quintic trajectory in Eq. (4.1), equivalence of the above integral to the quadratic form on the right hand side of Eq. (4.3) is shown in Appendix B, following an approach similar to the one in [3]. Here $\boldsymbol{K} = diag\{\boldsymbol{K}_1, \boldsymbol{K}_2, \dots, \boldsymbol{K}_N\}$ such that:

$$\boldsymbol{K}_k = \begin{bmatrix} 4800T^3 & 1440T^2 & \boldsymbol{0}_{1\times4} \\ 1440T^2 & 576T & \boldsymbol{0}_{1\times4} \\ \boldsymbol{0}_{4\times1} & \boldsymbol{0}_{4\times1} & \boldsymbol{0}_{4\times4} \end{bmatrix} \quad , \quad k = 1, 2, \dots, N \tag{4.4}$$

N segments require the solution of $6N$ coefficients. The way point constraints (i.e., segment initial and final positions) are determined by the hole locations; providing $2N$ equations. Velocity, acceleration, and jerk continuity make up $3(N-1)$ equations. Also, zero acceleration and jerk constraints are imposed at the very first and last holes, to allow easy solution of the looping and stitching trajectories. This yields another 4 equations. The initial and final velocity boundary conditions are left free, in order to allow connection at nonzero velocities. This leaves the problem of accelerating into and decelerating out of the cluster to the looping and stitching trajectories, which enables shorter segment durations (i.e., higher laser frequencies) to be achieved. In each axis, these constraints provide $5N+1$ equations which may be clustered in Eq. (4.5), as shown in Appendix B:

$$\boldsymbol{L}\boldsymbol{\theta}_i = \boldsymbol{\xi}_i \quad , \quad \text{where:} \quad i = x, y, z, a, c \tag{4.5}$$

Above, $\boldsymbol{L}\ ((5N+1)\times 6N)$ is solely a function of T and identical in all axes. $\boldsymbol{\xi}_i\ (6N\times 1)$, however, depends on the hole coordinates, which is typically different for each axis. Quadratic minimization of Eq. (4.3) subject to the constraints in Eq. (4.5) yields the following set of linear equations:

$$\begin{bmatrix} \boldsymbol{K} & \boldsymbol{L}^T \\ \boldsymbol{L} & \boldsymbol{0} \end{bmatrix} \cdot \begin{bmatrix} \boldsymbol{\theta}_i \\ \boldsymbol{\Lambda}_i \end{bmatrix} = \begin{bmatrix} \boldsymbol{0} \\ \boldsymbol{\xi}_i \end{bmatrix} \quad , \quad \text{for} \quad i = x, y, z, a, c \tag{4.6}$$

Above, $\boldsymbol{\Lambda}_i$ contains the Lagrange Multipliers to enforce continuity and boundary condition constraints. The minimum snap trajectory is obtained by solving $\boldsymbol{\theta}_x, \boldsymbol{\theta}_y, \boldsymbol{\theta}_z, \boldsymbol{\theta}_a$ and $\boldsymbol{\theta}_c$.

The full mathematical derivation of the minimum-snap quintic trajectory can be found in Appendix B.

4.3 Step 2: Time Scaling

If the initial guess for T results in too short a travel time between consecutive hole locations, then the axis velocity, acceleration, jerk, or x-y component of the part velocity at the hole location may become excessive and ultimately violate the limits in Eq. (3.4). On the other hand if T is chosen too large, then magnitudes of the kinematic profiles will be too small, thus under-utilizing the machine's true capabilities and process tolerances. In order to avoid either undesirable case, the second sub-step performs time scaling to bring all of the kinematic profiles within their limits, while minimizing the value of T.

Considering that the position profile can be expressed as a function of time (i.e., $x = f(t)$), scaling the time variable by α will modify the position profile to become $g(t) = f(t/\alpha)$. It can be analytically verified, as shown in Appendix C, that this will also scale the velocity, acceleration, and jerk profiles by $1/\alpha$, $1/\alpha^2$, and $1/\alpha^3$:

$$\dot{g}(t) = \frac{1}{\alpha}\dot{f}(t/\alpha)\ ,\ \ddot{g}(t) = \frac{1}{\alpha^2}\ddot{f}(t/\alpha)\ ,\ \dddot{g}(t) = \frac{1}{\alpha^3}\dddot{f}(t/\alpha) \tag{4.7}$$

Hence, the time scaling required to ensure that all velocity profiles remain within their limits in Eq. (3.4) can be obtained as:

$$\alpha_{vel} = \left\| \left[\frac{\dot{x}(t)}{\dot{x}_{\max}} \quad \frac{\dot{y}(t)}{\dot{y}_{\max}} \quad \dots \quad \frac{\dot{c}(t)}{\dot{c}_{\max}} \quad \frac{v_{xy}(t)}{v_{xy,\max}} \right] \right\|_{\infty} \tag{4.8}$$

Above, $\|[\bullet]\|_{\infty}$ denotes the infinity norm (i.e., peak value) of the normalized velocity vector $[\bullet]$, considering all of its entries (i.e., normalized joint velocity values) over their time history [73]. A value for α_{vel} that is larger than 1 indicates that a velocity limit is violated in at least one of the axes, which can be corrected by scaling the segment duration by α_{vel} ($T' = \alpha_{vel} T$).

Considering the impact of time scaling on the acceleration and jerk profiles, as indicated in Eq. (4.7), the time scaling required to bring the acceleration (α_{acc}) and jerk (α_{jerk}) profiles within their limits can be obtained as:

$$\left.\begin{aligned} \alpha_{acc} &= \left\| \left[\frac{\ddot{x}(t)}{\ddot{x}_{\max}} \quad \frac{\ddot{y}(t)}{\ddot{y}_{\max}} \quad \frac{\ddot{z}(t)}{\ddot{z}_{\max}} \quad \frac{\ddot{a}(t)}{\ddot{a}_{\max}} \quad \frac{\ddot{c}(t)}{\ddot{c}_{\max}} \right] \right\|_{\infty}^{1/2} \\ \alpha_{jerk} &= \left\| \left[\frac{\dddot{x}(t)}{\dddot{x}_{\max}} \quad \frac{\dddot{y}(t)}{\dddot{y}_{\max}} \quad \frac{\dddot{z}(t)}{\dddot{z}_{\max}} \quad \frac{\dddot{a}(t)}{\dddot{a}_{\max}} \quad \frac{\dddot{c}(t)}{\dddot{c}_{\max}} \right] \right\|_{\infty}^{1/3} \end{aligned}\right\} \tag{4.9}$$

Hence, the overall time scaling required to hold all of the constraints in Eq. (3.4), with at least one of the kinematic profiles reaching its maximum allowed magnitude, can be obtained as:

$$\text{Time scaling factor: } \alpha = \left\| [\alpha_{vel} \quad \alpha_{acc} \quad \alpha_{jerk}] \right\|_{\infty} \tag{4.10}$$

After fitting the minimum snap trajectory, the profiles ($\dot{\boldsymbol{q}}, \ddot{\boldsymbol{q}}, \dddot{\boldsymbol{q}}, v_{xy}$) are evaluated, using typically 5 points per segment, and the required time scaling α is computed from Eqs. (4.8)-(4.10). The segment duration and quintic coefficients are then updated as:

$$\left.\begin{aligned} &T' = \alpha T \\ &A'_{ik} = A_{ik} / \alpha^5, \; B'_{ik} = B_{ik} / \alpha^4, \; C'_{ik} = C_{ik} / \alpha^3 \\ &D'_{ik} = D_{ik} / \alpha^2, \; E'_{ik} = E_{ik} / \alpha, \; F'_{ik} = F_{ik} \end{aligned}\right\} \quad \begin{aligned} i &= x, y, z, \\ &a, c \end{aligned} \tag{4.11}$$

By the end of this sub-step, a feasible initial guess is guaranteed which satisfies all of the conditions in Eq. (3.4). The value of α calculated at this point will be '1', indicating that the

shortest possible segment duration has been reached for the trajectory shape parameterized so far.

4.4 Step 3: Profile Shape Optimization

The basic idea in this sub-step is to modify the shape of the quintic segments to enable the maximum possible reduction in the value of α (i.e. below '1'), which means that the segment duration T can be shortened further. This is done by modulating the axis velocity and acceleration boundary conditions at the hole locations, while keeping the segment duration constant. Since v_{xy} is influenced by simultaneous motion of x, y, a, and c-axes (Eq. (3.2)), the hole elongation constraint couples the optimization of profiles in these axes together. The z-axis can be either optimized independently, or alongside the other axes. The latter approach was taken here, mainly for programming convenience.

Given *0*th, *1*st and *2*nd order boundary conditions at hole *k*: $\boldsymbol{Q}_k = [X_k \ \dots \ C_k]^T$, $\dot{\boldsymbol{Q}}_k = [\dot{X}_k \dots \dot{C}_k]^T$, $\ddot{\boldsymbol{Q}}_k = [\ddot{X}_k \dots \ddot{C}_k]^T$, the objective is mathematically stated in Eq. (4.12), using the definition of α from Eqs. (4.8)-(4.10):

$$\min_{\boldsymbol{Q},\dot{\boldsymbol{Q}}} \alpha(\boldsymbol{Q},\dot{\boldsymbol{Q}},\ddot{\boldsymbol{Q}},T) \text{ where: } \begin{cases} \boldsymbol{Q} = [\boldsymbol{Q}_1^T \dots \boldsymbol{Q}_{N+1}^T]^T & : \text{ constant} \\ \dot{\boldsymbol{Q}} = [\dot{\boldsymbol{Q}}_1^T \dots \dot{\boldsymbol{Q}}_{N+1}^T]^T & : \text{ variable} \\ \ddot{\boldsymbol{Q}} = [\ddot{\boldsymbol{Q}}_2^T \dots \ddot{\boldsymbol{Q}}_N^T]^T & : \text{ variable} \end{cases} \tag{4.12}$$

As previously noted in Section 4.2, the initial and final velocity boundary conditions ($\dot{\boldsymbol{Q}}_1, \dot{\boldsymbol{Q}}_{N+1}$) are left as free variables to allow entry into and exit out of the cluster at high speeds. The acceleration boundary conditions ($\ddot{\boldsymbol{Q}}_1, \ddot{\boldsymbol{Q}}_{N+1}$) are set to zero and excluded from the optimization to simplify the solution of the connecting looping and stitching trajectories, by relieving the requirement to match nonzero acceleration boundary conditions. Trials conducted by also optimizing these boundary conditions revealed no significant improvement in the achievable time reduction. In the practical implementation, $\dot{\boldsymbol{Q}}$ and $\ddot{\boldsymbol{Q}}$ are also normalized by their maximum allowable magnitudes to facilitate better convergence.

The most significant merit of Eq. (4.12) is that the nonlinear constrained optimization problem originally stated in Eqs. (3.4)-(3.5) is now transformed into an *unconstrained* problem, using the definition of α which implicitly contains the constraints. Hence, the

optimization can be efficiently carried out using well-proven techniques for unconstrained problems, such as the Quasi-Newton method [55]. The objective function weighs each constraint based on its relative impact on the achievable time reduction and focuses the on the most critical parts of the trajectory. One difficulty, however, is that the ∞-norm operator picks out the single worst case (i.e., peak magnitude) value among all of its entries. Hence, when there are multiple critical points in the profiles that yield similarly high values for α, such discriminatory behaviour can result in these points being chosen as the 'worst-case' one after another. Obviously, this can cause discontinuity when evaluating the gradient of the objective during successive iterations, thereby hampering convergence. As a practical work around, the ∞-norm is replaced with the more general *p*-norm, defined as [73]:

$$\left\| \boldsymbol{b}_{1\times n} \right\|_p \overset{def}{=} \left\| \begin{bmatrix} b_1 & \dots & b_n \end{bmatrix} \right\|_p = \left[\sum_{k=1}^{n} \left| b_k \right|^p \right]^{1/p} \quad , \quad \boldsymbol{b} \in \Re^{1xn} \tag{4.13}$$

Hence, the expression for α in the objective function now becomes smooth, which can be verified by combining Eqs. (4.8)-(4.10) and (4.13) to be:

$$\alpha = \left\{ \begin{array}{c} \sum_{k=1}^{n} \left(\left| \frac{\dot{x}(k)}{\dot{x}_{\max}} \right|^p + \dots + \left| \frac{\dot{c}(k)}{\dot{c}_{\max}} \right|^p + \left| \frac{v_{xy}(k)}{v_{xy,\max}} \right|^p \right) + \left[\sum_{k=1}^{n} \left(\left| \frac{\ddot{x}(k)}{\ddot{x}_{\max}} \right|^p + \dots + \left| \frac{\ddot{c}(k)}{\ddot{c}_{\max}} \right|^p \right) \right]^{1/2} \\ + \left[\sum_{k=1}^{n} \left(\left| \frac{\dddot{x}(k)}{\dddot{x}_{\max}} \right|^p + \dots + \left| \frac{\dddot{c}(k)}{\dddot{c}_{\max}} \right|^p \right) \right]^{1/3} \end{array} \right\}^{1/p} \tag{4.14}$$

Above, k is the discrete sample index and n denotes the total number of samples used in evaluating each profile. Just as α is a smooth function of the velocity, acceleration, and jerk profiles, these profiles are also smooth functions of the spline coefficients, and therefore the *0*th, *1*st, and *2*nd order boundary conditions, per Eqs. (4.1)-(4.2). Shape optimization is conducted in 3 runs, during which the value of p evolves from 10 to 100 to 1000. Each run uses the result of the previous one as its initial guess. The first run tries to push the kinematic profiles away from their limits as a whole, while placing greater emphasis on the critical portions close to the limits. The gradients are continuous and convergence to a sub-optimal solution is quick. Afterwards, consecutive runs focus on the critical portions. It was observed that applying this gradual transition rather than directly using the ∞-norm from the beginning reduces the computational time by typically 30% for clusters with 100 or more way points.

Once the optimized *1*st and *2*nd order boundary conditions are determined, the corresponding quintic spline coefficients can be calculated using Eq. (4.2). By the end of this sub-step, the maximum amount of 'wiggle room' is recovered in the profiles, which enables further reduction of the segment travel period. Although globality of this minimum is not guaranteed, this step typically provides a substantial improvement in the achievable cycle time reduction.

4.5 Step 4: Final Time Adjustment

After shape optimization, the achieved value of α is used to scale the quintic segments again using Eq. (4.11). Although each cluster allows a different laser frequency to be achieved, it may not always be practical to alter the pulsing period amid the part program. Especially latencies in the laser control circuitry, which can be as large as tens of seconds when performing a recipe change, can negate any cycle time improvement gained by careful trajectory optimization. Hence, after all of the clusters are optimized, the lowest achievable laser pulsing frequency is adopted throughout the part program and all of the spline segments are updated one last time using Eq. (4.11).

4.6 Conclusion

This chapter has provided the details of the proposed trajectory optimization algorithm for hole clusters. The technique guarantees a feasible solution and uses a novel re-formulation of the optimization problem, which transforms it from a constrained minimization problem to an unconstrained one. In numerical implementation, this approach was found to converge significantly (up to 80%) faster, and also yield 40-50% shorter cycle time compared to applying direct constrained optimization using sequential quadratic programming.

The following chapters will present the proposed time-optimized solution for connecting optimized cluster trajectories together.

Chapter 5

Time-Optimal Looping and Stitching

5.1 Introduction

This chapter presents a stitching algorithm for looping the same cluster trajectory (for multiple drilling passes) and stitching between consecutive clusters. For point to point motion the 's-curve' profile shown in Figure 5.1 is known to be the time-optimal one. Here, this approach has been adopted with some modification, which generates the quickest possible motion for each axis with guaranteed kinematic feasibility, as presented in Section 5.2. Then, all axes need to be synchronized so that the total motion duration is equal to that of the slowest axis, and an integer multiple of the laser pulsing period, which is explained in Section 5.3. This is done to avoid turning the laser off while repositioning the beam, which can result in tens of seconds in the laser control circuitry. Instead, a quick shutter is used in the optics path, which diverts the beam away from the workpiece. Slowing down the profiles in the faster axes allows for a wide range of feasible solutions to choose from, which is utilized to the advantage of reducing the vibrations induced by minimizing the motion jerk in the individual axes, as explained in Section 5.4. The trajectories that are planned for each axis with different switching times are then assembled and re-parameterized, so they can be executed as a single continuous stream. Details of this step are presented in Section 5.5, which also shows a sample result for the overall stitching algorithm developed in this chapter. Finally, the conclusions are presented in Section 5.6.

5.2 Time Optimal Solution for Individual Axes

In the general case, s-curve motion may contain up to 7 segments comprising of 2 acceleration regions ①-③, ⑤-⑦ and possibly a constant velocity region ④. Although the initial and final boundary conditions ((x_1, v_1) and (x_8, v_8)) are given, the intermediate velocity (v_4) is not known ahead of time. The overall profile also has to satisfy the following displacement condition ($\Delta x = x_8 - x_1$):

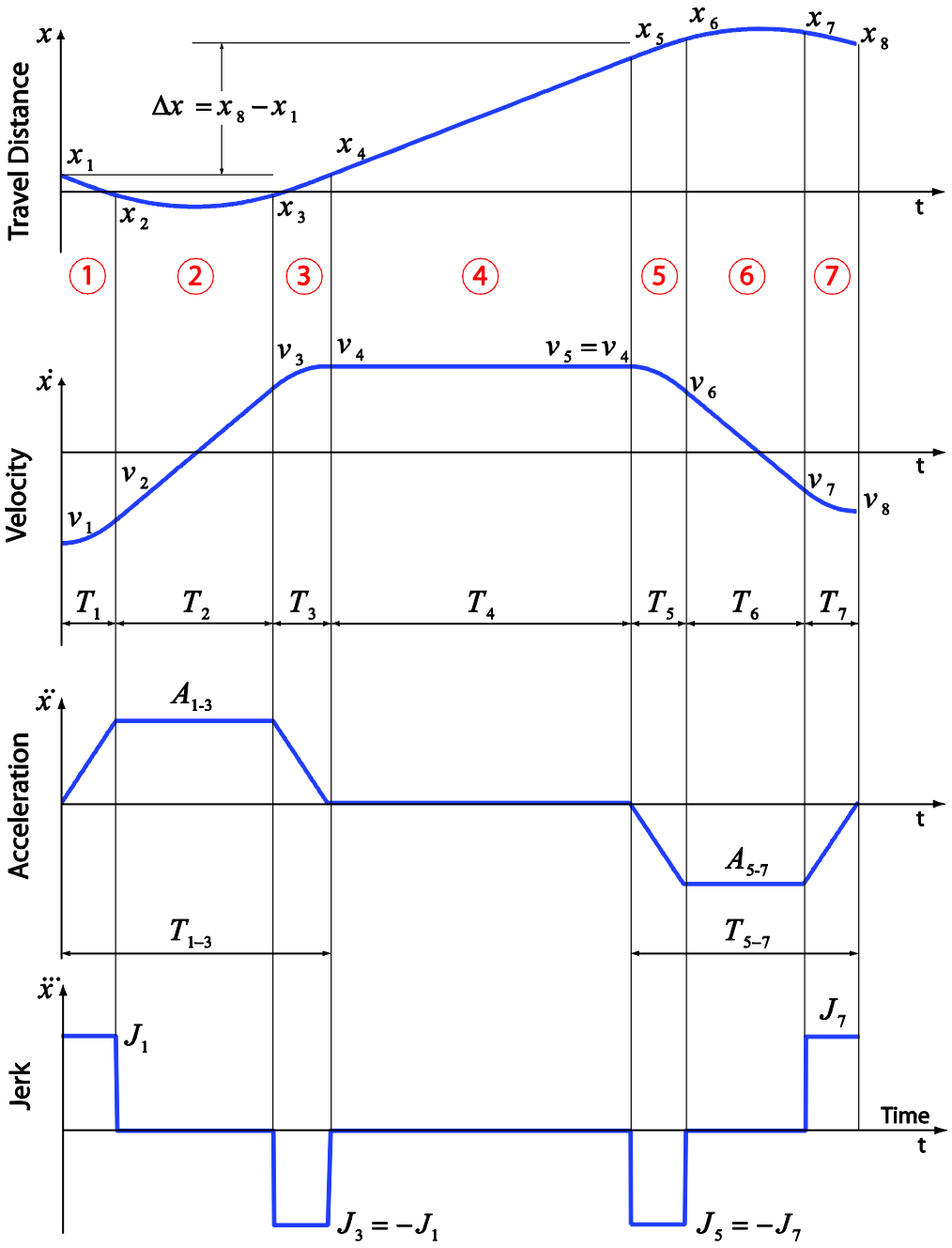

Figure 5.1: Trapezoidal Acceleration Profile for a Single Axis used in Generating the Looping and Stitching Trajectories

$$\Delta x = \underbrace{\frac{v_1 + v_4}{2}\left(T_1 + T_2 + T_3\right)}_{\text{Segments (1)-(3)}} + \underbrace{v_4 T_4}_{\substack{\text{Const.} \\ \text{Vel. (4)}}} + \underbrace{\frac{v_4 + v_8}{2}\left(T_5 + T_6 + T_7\right)}_{\text{Segments (5)-(7)}} \tag{5.1}$$

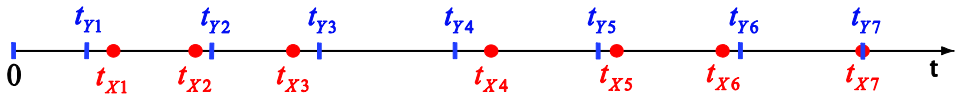

Figure 5.2: Transition Times in x- and y- Axes

The time-optimal trajectory is solved by scanning v_4 within its limits, while also considering the cases $v_4 = v_1$ and $v_4 = v_8$. The acceleration demand for each solution is evaluated from,

$$\left.\begin{aligned} A_{1-3} &= \mathrm{sgn}(v_4 - v_1)\sqrt{J_{\max}\left|v_4 - v_1\right|} \;\rightarrow\; T_1 = T_3 = \left|A_{1-3}\right| / J_{\max} \\ A_{5-7} &= \mathrm{sgn}(v_8 - v_4)\sqrt{J_{\max}\left|v_8 - v_4\right|} \;\rightarrow\; T_5 = T_7 = \left|A_{5-7}\right| / J_{\max} \end{aligned}\right\} \tag{5.2}$$

Above, $J_{\max}$ is the axis jerk limit. If the magnitudes of A_{1-3} or A_{5-7} exceed their limit ($A_{\max}$), they are capped by this value and the necessary constant acceleration duration (T_2 and T_6) is computed (which would otherwise be zero), while also updating the jerk durations:

$$\left.\begin{aligned} T_2 &= \frac{|v_4 - v_1|}{A_{\max}} - \frac{A_{\max}}{J_{\max}} \quad , \quad T_1 = T_3 = \frac{A_{\max}}{J_{\max}} \\ T_6 &= \frac{|v_8 - v_4|}{A_{\max}} - \frac{A_{\max}}{J_{\max}} \quad , \quad T_5 = T_7 = \frac{A_{\max}}{J_{\max}} \end{aligned}\right\} \tag{5.3}$$

From the above calculations, if $v_4 \neq 0$, the constant velocity duration T_4 can be computed using Eq. (5.1) as,

$$T_4 = \frac{1}{v_4}\left\{\Delta x - \left(\frac{v_1 + v_4}{2}\left(T_1 + T_2 + T_3\right)\right) - \left(\frac{v_4 + v_8}{2}\left(T_5 + T_6 + T_7\right)\right)\right\} \tag{5.4}$$

Otherwise, T_4 is set to zero. The total motion time required for a single axis is then calculated as $T_{tot} = \sum_{k=1}^{7} T_k$. The solution that yields the smallest value for T_{tot} while holding $T_4 \geq 0$ is chosen as the time-optimal one for the axis under consideration.

5.3 Synchronization of Multiple Axes

After computing the fastest profile for each axis, all axes are synchronized so that the total looping or stitching duration is equal to that of the slowest axis, and is an integer multiple of the laser pulsing period. This concept is illustrated for the x- and y-axes in Figure

5.2, which shows that in spite of different switching times for the jerk transition periods, the two axes complete the motion at the same time (i.e. $t_{X7} = t_{Y7}$). However, it is not possible to just scale the time variable for the faster axes, as this would also shift the velocity boundary conditions. Instead, the profiles need to be re-solved to satisfy ***both the travel displacement*** and ***motion duration conditions***, in addition to satisfying the given position and velocity boundary conditions and velocity, acceleration and jerk limits. This is done by re-planning the faster axes to minimize the integral square of jerk, as explained in Section 5.4.

5.4 Motion Re-planning for Minimal Jerk

The motion in the faster axes is re-planned to have the same total duration with the slowest axis: T_{tot}. Considering the given boundary conditions, and velocity, acceleration, and jerk limits, three are four possible kinematic solutions in each axis, which take the forms illustrated in Figure 5.3.

For each case, the feasible solutions are investigated by scanning different values for the intermediate velocity value (v_4). Afterwards, the feasible solution that yields the lowest value for the integral square of jerk is chosen. The objective to be minimized can be expressed as:

$$\int_0^{T_{tot}} J^2 dt = \int_0^{T_1} J_1^2 dt + \int_0^{T_3} J_3^2 dt + \int_0^{T_5} J_5^2 dt + \int_0^{T_7} J_7^2 dt \tag{5.5}$$

Considering that $|J_1| = |J_3| = |J_5| = |J_7| = J$, and also $T_1 = T_3$ and $T_5 = T_7$, the minimum jerk objective becomes,

$$Min\ Jerk\ Objective = J^2(T_1 + T_3 + T_5 + T_7) = 2J^2(T_1 + T_5) \tag{5.6}$$

The solutions for each case are detailed in the following:

Case #1: In this case $T_2 = 0$, $T_6 = 0$, $|A_1| \le A_{\max}$, and $|A_5| \le A_{\max}$. It is necessary to hold Δx (Eq. (5.1)) and T_{tot}:

$$T_{tot} = T_1 + T_2 + T_3 + T_4 + T_5 + T_6 + T_7 = 2T_1 + T_4 + 2T_5 \tag{5.7}$$

From the triangular shape of the acceleration transients, T_1 and T_5 can be expressed as:

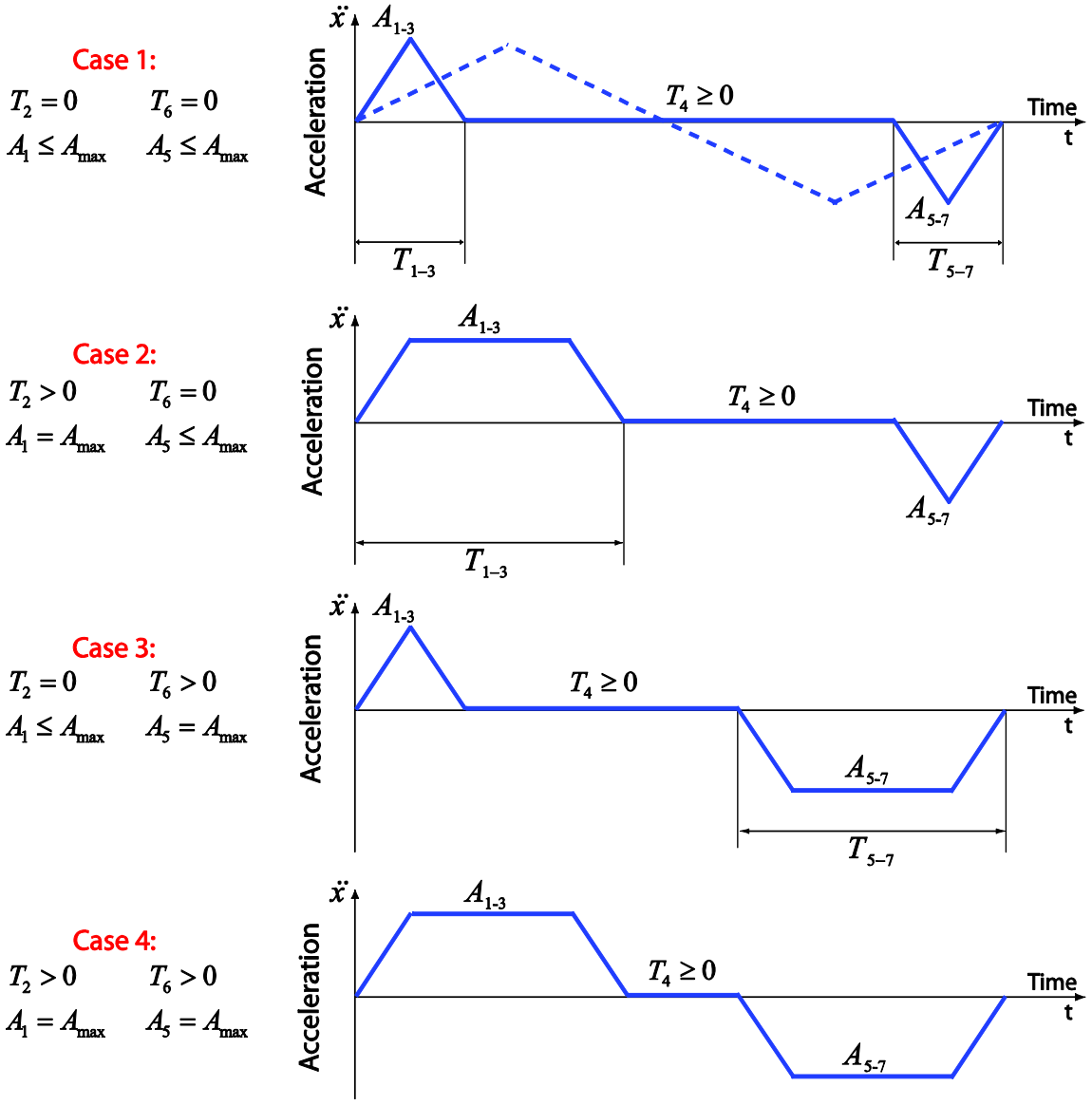

Figure 5.3: Four Different Cases for Trapezoidal Acceleration Profile

$$T_1 = T_3 = \frac{|A_1|}{J} = \frac{\sqrt{|v_4 - v_1|}}{\sqrt{J}} \quad , \quad T_5 = T_7 = \frac{|A_5|}{J} = \frac{\sqrt{|v_8 - v_4|}}{\sqrt{J}} \tag{5.8}$$

Substituting these into the total displacement and time expressions in Eq. (5.1) and (5.7), the values for J and T_4 can be solved as:

$$J = \left[\frac{(v_1 - v_4)\sqrt{|v_4 - v_1|} + (v_8 - v_4)\sqrt{|v_8 - v_4|}}{\Delta x - v_4 T_{tot}} \right]^2$$
$$T_4 = T_{tot} - \frac{2\sqrt{|v_4 - v_1|} + 2\sqrt{|v_8 - v_4|}}{\sqrt{J}} \tag{5.9}$$

Simultaneous realization of $T_4 \geq 0$ and $0 \leq J \leq J_{\max}$ indicates the feasibility of the tried value for v_4.

Case #2: In this case $T_2 > 0$ ($|A_1| = A_{\max}$), $T_6 = 0$ ($|A_5| \leq A_{\max}$). Again, Eqs. (5.1) and (5.7) need to hold. While the expression for T_5 in Eq. (5.8) still holds, due to the trapezoidal shape of the first acceleration transient, which assumes a maximum magnitude of $A_{\max}$, T_1, T_2, and T_5 take the form:

$$T_1 = T_3 = \frac{A_{\max}}{J} \qquad T_2 = \frac{|v_4 - v_1|}{A_{\max}} - \frac{A_{\max}}{J} \qquad T_5 = T_7 = \frac{\sqrt{|v_8 - v_4|}}{\sqrt{J}} \tag{5.10}$$

Substituting these into Eqs. (5.1) and (5.7) yields:

$$T_4 = T_{tot} - \frac{|v_4 - v_1|}{A_{\max}} - \frac{A_{\max}}{J} - \frac{2\sqrt{|v_8 - v_4|}}{\sqrt{J}} \tag{5.11}$$

$$\underbrace{\frac{(v_1 - v_4)A_{\max}}{2}}_{\alpha}\left(\frac{1}{\sqrt{J}}\right)^2 + \underbrace{(v_8 - v_4)\sqrt{|v_8 - v_4|}}_{\beta}\frac{1}{\sqrt{J}} + \underbrace{(v_4 T_{tot} - \frac{(v_4 - v_1)|v_4 - v_1|}{2A_{\max}} - \Delta x)}_{\gamma} = 0 \tag{5.12}$$

The roots of the quadratic expression in Eq. (5.12) are inspected and the values for v_4 which yield $T_4 \geq 0$ and $0 \leq J \leq J_{\max}$ (with $J \in \Re$) are considered as feasible solutions.

Case #3: In this case $T_2 = 0$ ($|A_1| \leq A_{\max}$), $T_6 > 0$ ($|A_5| = A_{\max}$). While the expression for T_1 in Eq. (5.8) holds, due to the trapezoidal shape of the second acceleration transient, which assumes a maximum magnitude of $A_{\max}$, T_1, T_5, and T_6 take the form:

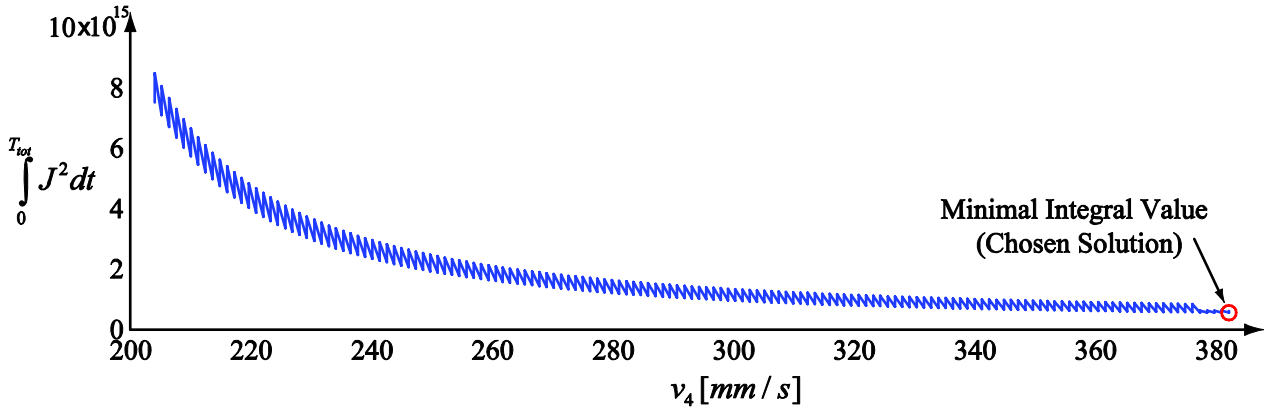

Figure 5.4: Integral Square of Jerk for Different Feasible v_4 Solutions

$$T_1 = T_3 = \frac{\sqrt{|v_4 - v_1|}}{\sqrt{J}} \qquad T_5 = T_7 = \frac{A_{\max}}{J} \qquad T_6 = \frac{|v_8 - v_4|}{A_{\max}} - \frac{A_{\max}}{J} \tag{5.13}$$

Substituting these into Eqs. (5.1) and (5.7) yields:

$$T_4 = T_{tot} - \frac{2\sqrt{|v_4 - v_1|}}{\sqrt{J}} - \frac{|v_8 - v_4|}{A_{\max}} - \frac{A_{\max}}{J} \tag{5.14}$$

$$\underbrace{\frac{(v_8 - v_4)A_{\max}}{2}}_{\alpha}\left(\frac{1}{\sqrt{J}}\right)^2 + \underbrace{(v_1 - v_4)\sqrt{|v_4 - v_1|}}_{\beta}\frac{1}{\sqrt{J}} + \underbrace{(v_4 T_{tot} - \frac{(v_4 - v_8)\,|v_8 - v_4|}{2A_{\max}} - \Delta x)}_{\gamma} = 0 \tag{5.15}$$

The feasibility of each solution, obtained by trying out a value of v_4 is checked in a manner similar to that of Case #2.

Case #4: In this case $T_2 > 0$ ($|A_1| = A_{\max}$), $T_6 > 0$ ($|A_5| = A_{\max}$). Therefore the time interval expressions assume the form:

$$T_1 = T_3 = \frac{A_{\max}}{J} \qquad T_2 = \frac{|v_4 - v_1|}{A_{\max}} - \frac{A_{\max}}{J} \qquad T_5 = T_7 = \frac{A_{\max}}{J} \qquad T_6 = \frac{|v_8 - v_4|}{A_{\max}} - \frac{A_{\max}}{J} \tag{5.16}$$

Substituting these into Eqs. (5.1) and (5.7) yields:

$$J = \frac{(v_1 - 2v_4 + v_8)A_{\max}^2}{2A_{\max}(\Delta x - v_4 T_{tot}) + (v_4 - v_1)|v_4 - v_1| + (v_4 - v_8)|v_8 - v_4|} \tag{5.17}$$

$$T_4 = T_{tot} - \frac{|v_4 - v_1| + |v_8 - v_4|}{A_{\max}} - \frac{2A_{\max}}{J} \tag{5.18}$$

Simultaneous realization of $0 \le J \le J_{\max}$ and $T_4 \ge 0$ indicates the feasibility of the tried value for v_4.

Figure 5.4 shows an example of the sorted the values for the integral square of jerk calculated at different intermediate velocity (v_4) values. As can be seen, applying the minimum jerk criterion, when re-solving the trajectories for the faster axes, can lead to an order of magnitude reduction in the integral square of jerk, thereby resulting in smoother motion on the machine in overall.

After determining the overall time-optimal, and axis level jerk-optimal trajectory, the corresponding acceleration and jerk magnitudes are updated as follows:

$$\text{if } T_{1,\chi} > 0, \text{then}: \; A_{1,\chi} = \frac{v_{4,\chi} - v_{1,\chi}}{T_{1,\chi} + T_{2,\chi}}, \; J_{1,\chi} = \frac{v_{1,\chi}}{T_{1,\chi}} \quad \text{otherwise}, \; A_{1,\chi} = 0 \; , \; J_{1,\chi} = 0 \tag{5.19}$$

$$\text{if } T_{5,\chi} > 0, \text{then}: \; A_{5,\chi} = \frac{v_{8,\chi} - v_{4,\chi}}{T_{5,\chi} + T_{6,\chi}}, \; J_{5,\chi} = \frac{v_{5,\chi}}{T_{5,\chi}} \quad \text{otherwise}, \; A_{5,\chi} = 0 \; , \; J_{5,\chi} = 0 \tag{5.20}$$

5.5 Assembly of the Trajectories Generated for Different Axes

It should be noted that the segment boundaries (i.e., jerk switching times) will be different among the axes, as shown in Figure 5.2 for the x- and y-axes. This asynchronous behaviour is handled by chopping up the trajectory into smaller sub-segments with shorter durations marked by the switching times, resulting in a vector of switching instances that are sorted in sequence. (e.g. for Figure 5.2, $T = \{ t_{1y} \;\; t_{1x} \;\; t_{2x} \;\; t_{2y} \;\; t_{3x} \;\; t_{3y} \;\; t_{4y} \;\; t_{4x} \;\; t_{5y} \;\; t_{5x} \;\; t_{6x} \;\; t_{6y} \}$). Duplicate instances are eliminated, which can occur if two or more axes need to switch at the same time. Then, each new trajectory segment is parameterized to replicate the original optimized trajectory. Considering the illustration in Figure 5.5, the trajectory, starting at the beginning of the original segment can be expressed as:

$$x(t) = Ct^3 + Dt^2 + Et + F \tag{5.21}$$

Considering the relationship between the time variable (t) starting from the beginning of the original segment, and (τ), starting from the beginning of the newly formed segment:

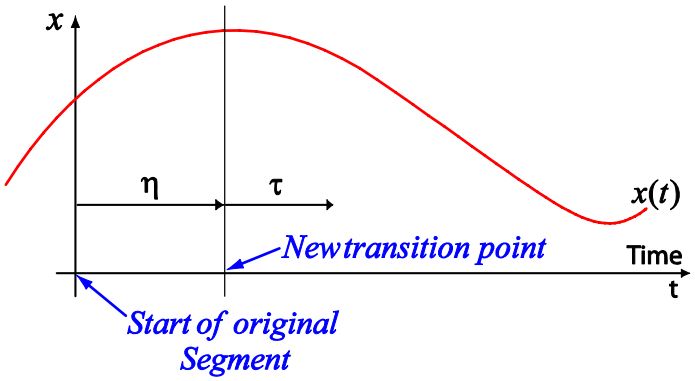

Figure 5.5: Trajectory Re-parameterization by Shifting the Beginning of the Segment

$$\tau = t - \eta \;\rightarrow\; t = \eta + \tau \qquad where \begin{cases} t^2 = \eta^2 + 2\eta\tau + \tau^2 \\ t^3 = \eta^3 + 3\eta^2\tau + 3\eta\tau^2 + \tau^3 \end{cases} \tag{5.22}$$

The same trajectory can be written in cubic form according to the beginning of the new segment as $x(\tau) = C'\tau^3 + D'\tau^2 + E'\tau + F'$, where:

$$\begin{aligned} x(\tau) &= C(\eta+\tau)^3 + D(\eta+\tau)^2 + E(\eta+\tau) + F \\ x(\tau) &= C(\eta^3 + 3\eta^2\tau + 3\eta\tau^2 + \tau^3) + D(\eta^2 + 2\eta\tau + \tau^2) + E(\eta+\tau) + F \\ x(\tau) &= \underbrace{C}_{C'}\tau^3 + \underbrace{(3C\eta + D)}_{D'}\tau^2 + \underbrace{(3C\eta^2 + 2D\eta + E)}_{E'}\tau + \underbrace{(C\eta^3 + D\eta^2 + E\eta + F)}_{F'} \end{aligned} \tag{5.23}$$

Afterwards, if a conversion to quintic polynomials is necessary, the fourth and fifth order coefficients (A' and B' terms) can be padded with zeros.

Sample results for the overall stitching/looping algorithm developed in chapter are shown in Figure 5.6. Here, the z-axis is the limiting axis, where the velocity, acceleration, and jerk limits are all reached while generating the time-optimal solution. Since the capabilities of the other axes do not need to be fully utilized, their solutions have been individually optimized to minimize the integral square of jerk. The motion starts and ends in all axes at the same time, and the given position and velocity boundary conditions are also respected, while achieving zero acceleration values at the beginning and end of the trajectory.

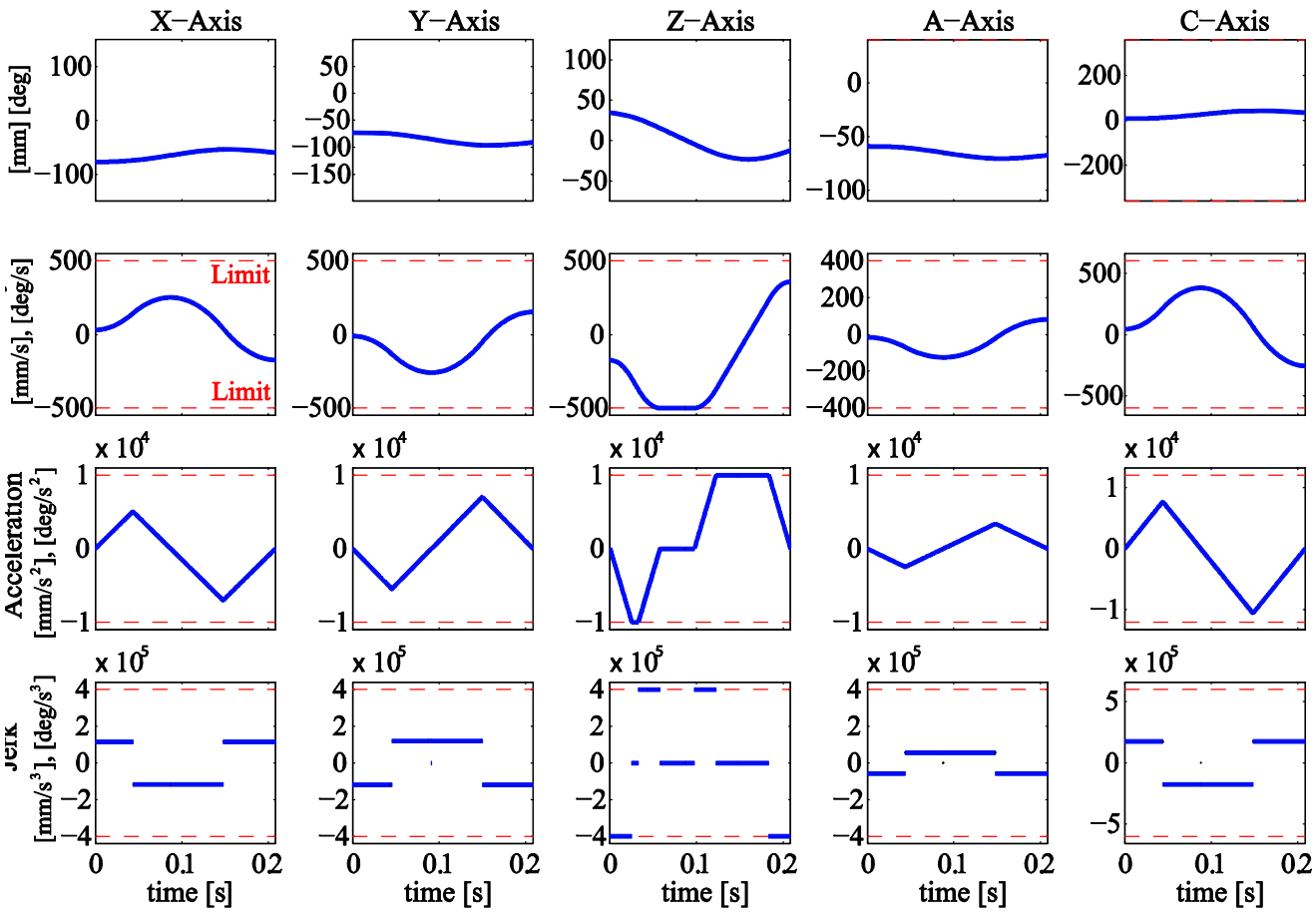

Figure 5.6: Kinematic Profiles Generated with the Stitching Algorithm Developed in this Chapter

5.6 Conclusion

This chapter has presented the solution for generating time- and jerk-optimal looping and stitching segments. The time optimal solution in each axis is individually obtained and the slowest axis, which requires the longest motion duration, becomes the bottleneck. Motion in the faster axes is re-planned to start and end simultaneously with the trajectory of the slowest axis. This re-planning also allows for an extra degree of optimization to be applied, which has been chosen as the minimization of the integral square of jerk, in order to facilitate smoother motion on the laser drilling machine, with less vibration on the laser optics. Handling of the asynchronous switching behaviour between different axes is also realized, by chopping up the trajectory into smaller segments, and parameterizing each segment according to the time offset from its original starting instance. Effectiveness of the overall stitching algorithm has been demonstrated with a numerical example.

The following chapter will utilize the cluster optimization algorithm and time-optimal looping/stitching algorithms developed in the previous and current chapters, to generate an on-the-fly laser drilling trajectory for an aerospace component, which is time-optimal for the given machine and process limits.

Chapter 6

Implementation Results

6.1 Introduction

The developed algorithms in this thesis have been applied on different gas turbine combustion chamber panels. The major result comparison in this chapter is between on-the-fly laser drilling and percussion drilling (stopping at each hole location to fully drill by pulsing a set number of times and complete the hole drilling process). To simplify the findings, only three panels to be laser drilled are explained in detail. The time-optimized trajectory behaviour is also shown for the three different aerospace panels. Figure 6.1 shows the three different hole patterns to be laser drilled.

6.2 Results

Sample implementation results for a gas turbine combustion chamber are shown in Figures 6.2-6.4. The developed algorithm has been used to generate a time-optimized trajectory for on-the-fly laser drilling of the hole locations in Clusters #1-#10 in Figure 1.2. The process and machine limits considered are also depicted in Figures 6.2-6.4. The trajectory was planned to allow each cluster to be repeated once before connecting to the next one. Among all clusters, the slowest segment period was obtained for Cluster #1, which corresponded to 8.1 Hz laser pulsing frequency (Table 6.1). Since the laser is programmable in integer frequencies, this was rounded down to 8 Hz (T = 0.125 s) and applied throughout the part program.

From the kinematic profiles, it can be seen that the velocity, acceleration, and jerk capabilities of x-, y-, z-, and c-axes are well utilized. Limits for axis-c are reached several times. The zoomed views, which show Cluster #2, indicate that the commands are indeed continuous up to acceleration level and limited in jerk. The x-y component of the part velocity shows that the hole elongation constraint is always respected, while in between the holes much higher velocities can be reached for speeding up the process (This limit is given by the manufacturer, or can be obtained using the duration of laser pulse and hole elongation limit). For a single pass, compared to linear interpolation which stops at the holes, the proposed technique provides over 6%

reduction in cycle time (Table 6.1-6.6), and more importantly 56% reduction in the integral square of jerk, which allows the process speed to be pushed up further without vibrating the optics. The optimized trajectories are streamed as fine point data to the Fanuc 30i controller in inverse time feed mode to preserve timing information. Preliminary experiments conducted on the laser machine tool at Pratt & Whitney Canada have validated the practicality and effectiveness of this scheme and further testing and integration is now underway. Such preliminary tests showed that the developed time-optimized trajectories did reduce the drilling time significantly (as tabulated in this Chapter) and reduced machine and laser optics vibrations noticeably, to the personnel's perception. This minimization in vibrations transmitted to laser optics significantly reduces the maintenance time required to realign the laser optics. Therefore, this thesis also reduces the overall drilling cost of turbine engine combustion chamber panels through minimizing the overall downtime of the drilling machine.

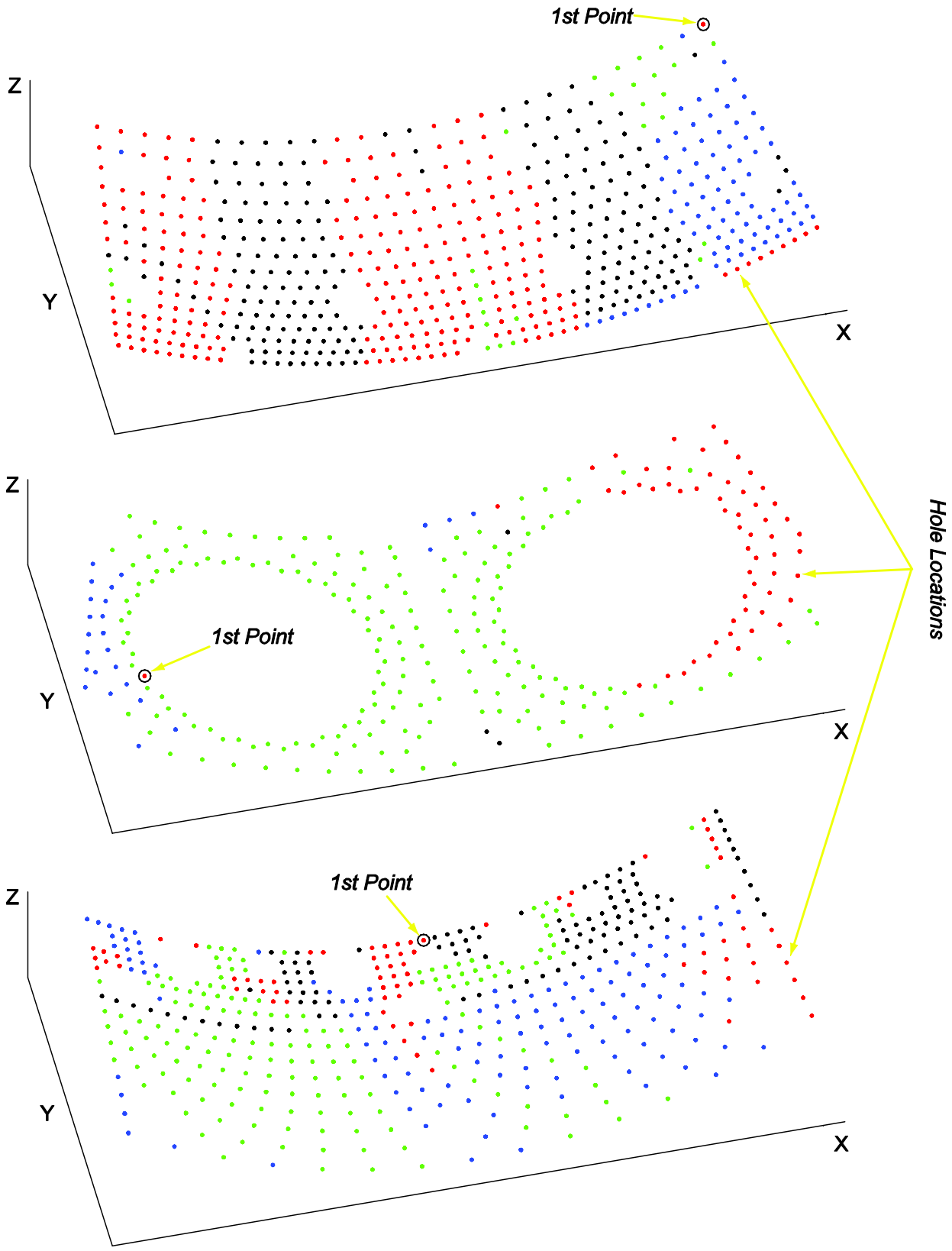

Figure 6.1: Three Different Examples of Turbine Engine Combustion Chamber Panels to Be Laser Drilled [Examples #1 - #3]

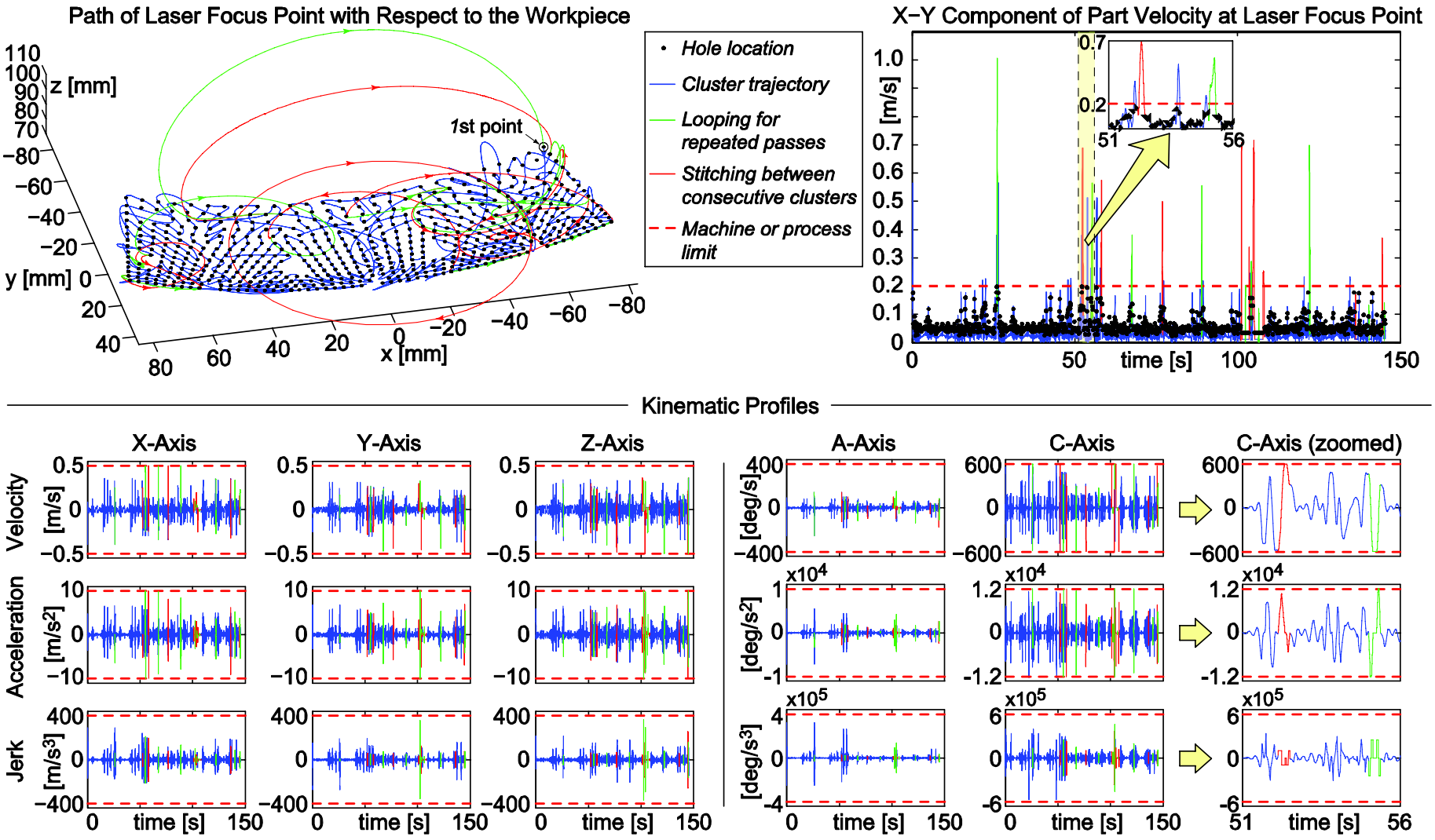

Figure 6.2: Implementation Results for a Gas Turbine Combustion Chamber Panel [Example #1]

Table 6.1: Cycle Time Comparison between the Optimized Spline Trajectory and Linear Interpolation with Full Stops through Consecutive Holes (assuming 1 laser shot per hole) [Example #1]

Cluster #	No. Of Points	Achievable Laser Frequency [Hz]	Used Laser Frequency [Hz]	Motion Duration [s]
1	208	**8.1035**	8.00	25.875
2	21	9.9831	8.00	2.500
3	73	11.6446	8.00	9.000
4	96	10.3931	8.00	11.875
5	9	152.9022	8.00	1.000
6	4	10.6034	8.00	0.375
7	10	133.5358	8.00	1.125
8	111	11.4109	8.00	13.750
9	32	10.8403	8.00	3.875
10	3	11.1027	8.00	0.250
Total:	**567**			**69.625**

Stitching Between Clusters	Motion Duration [s]
1→2	0.375
2→3	0.375
3→4	0.375
4→5	0.375
5→6	0.250
6→7	0.625
7→8	0.500
8→9	0.250
9→10	0.375
Total:	**3.500**

Total Duration for Clusters & Stitching [s]:
69.625 + 3.500 = **73.125**

Total Duration for Linear Interpolation (w/ full stops) [s]
77.250

[%] Time Reduction over Applying Linear Interpolation
5.34%

Table 6.2: Integral Square of Acceleration and Jerk Comparison between the Optimized Spline Trajectory and Linear Interpolation with Full Stops [Example #1]

Time Integral Square of Acceleration					
	X-Axis [mm^2/s^3]	Y-Axis [mm^2/s^3]	Z-Axis [mm^2/s^3]	A-Axis [deg^2/s^3]	C-Axis [deg^2/s^3]
Linear Interp.	1.34E+08	1.07E+08	2.17E+08	8.23E+06	3.43E+08
Spline Interp.	9.92E+07	7.02E+07	1.18E+08	1.36E+07	2.96E+08
Ratio (spline/linear)	74%	66%	54%	165%	86%
RMS Ratio (between the axes)		98%	Reduction		2%

Time Integral Square of Jerk					
	X-Axis [mm^2/s^5]	Y-Axis [mm^2/s^5]	Z-Axis [mm^2/s^5]	A-Axis [deg^2/s^5]	C-Axis [deg^2/s^5]
Linear Interp.	3.21E+11	2.60E+11	5.52E+11	1.96E+10	7.56E+11
Spline Interp.	6.41E+10	3.97E+10	5.94E+10	1.81E+10	1.69E+11
Ratio (spline/linear)	20%	15%	11%	92%	22%
RMS Ratio (between the axes)		44%	Reduction		56%

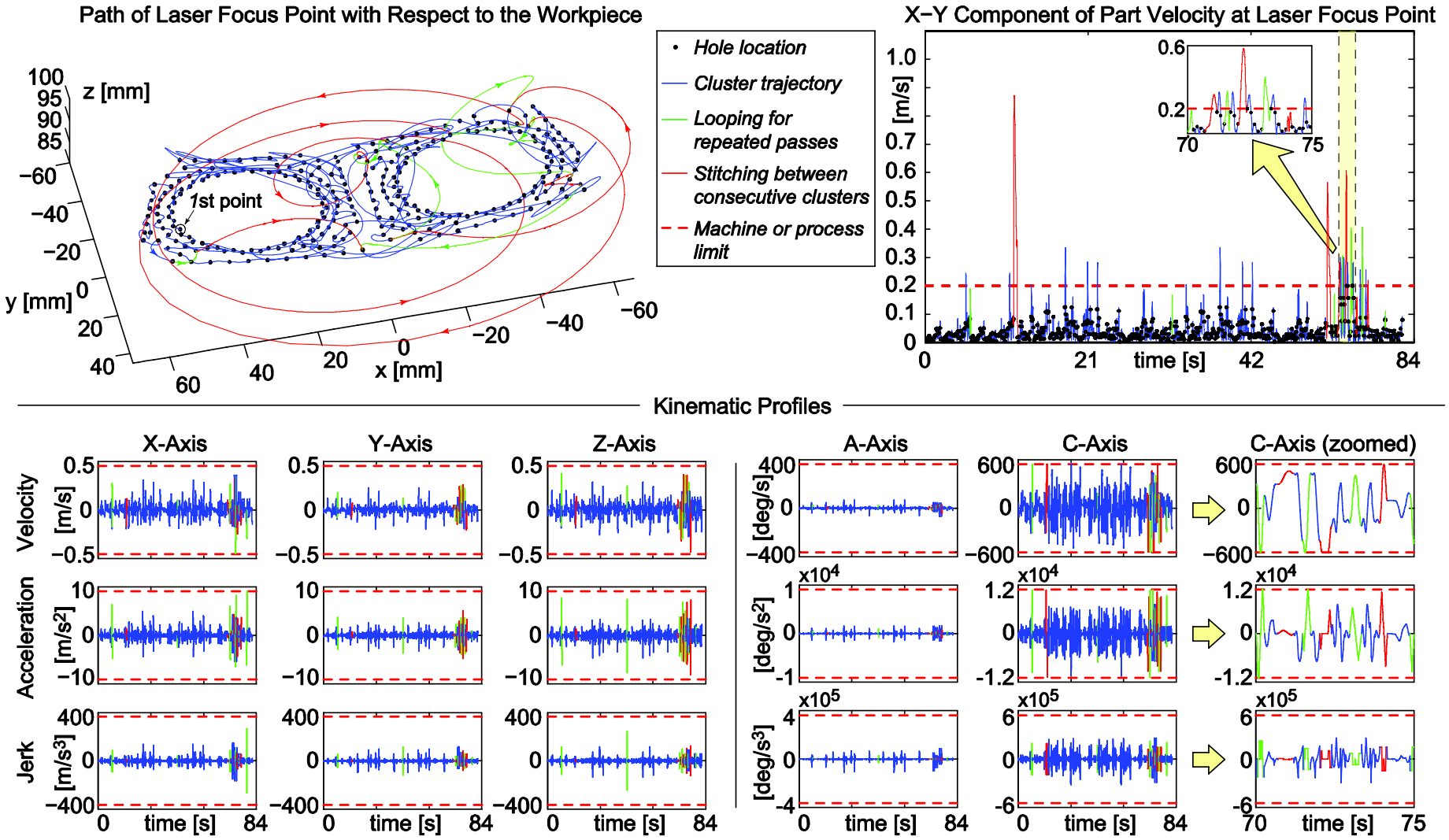

Figure 6.3: Implementation Results for a Gas Turbine Combustion Chamber Panel [Example #2]

Table 6.3: Cycle Time Comparison between the Optimized Spline Trajectory and Linear Interpolation with Full Stops through Consecutive Holes (assuming 1 laser shot per hole) [Example #2]

Cluster #	No. Of Points	Achievable Laser Frequency [Hz]	Used Laser Frequency [Hz]	Motion Duration [s]
1	52	12.5354	7.00	7.286
2	187	**7.0331**	7.00	26.571
3	4	12.8865	7.00	0.428
4	3	8.8729	7.00	0.286
5	5	8.9156	7.00	0.571
6	6	11.4755	7.00	0.714
7	21	14.0305	7.00	2.857
Total:	**278**			**39.253**

Stitching Between Clusters	Motion Duration [s]
1→2	0.750
2→3	0.750
3→4	0.500
4→5	0.375
5→6	0.250
6→7	0. 250
Total:	**2.875**

Total Duration for Clusters & Stitching [s]:
39.253 + 2.875 = **42.128**

Total Duration for Linear Interpolation (w/ full stops) [s]
43.250

[%] Time Reduction over Applying Linear Interpolation
2.59%

Table 6.4: Integral Square of Acceleration and Jerk Comparison between the Optimized Spline Trajectory and Linear Interpolation with Full Stops [Example #2]

Time Integral Square of Acceleration					
	X-Axis [mm^2/s^3]	Y-Axis [mm^2/s^3]	Z-Axis [mm^2/s^3]	A-Axis [deg^2/s^3]	C-Axis [deg^2/s^3]
Linear Interp.	7.47E+07	3.28E+07	9.74E+07	8.70E+05	4.25E+08
Spline Interp.	3.64E+07	1.86E+07	5.07E+07	2.81E+06	2.28E+08
Ratio (spline/linear)	49%	57%	52%	323%	54%
RMS Ratio (between the axes)		152%	Reduction		-52%

Time Integral Square of Jerk					
	X-Axis [mm^2/s^5]	Y-Axis [mm^2/s^5]	Z-Axis [mm^2/s^5]	A-Axis [deg^2/s^5]	C-Axis [deg^2/s^5]
Linear Interp.	1.71E+11	7.45E+10	2.23E+11	2.10E+09	8.96E+11
Spline Interp.	1.68E+10	1.11E+10	2.10E+10	4.02E+09	1.25E+11
Ratio (spline/linear)	10%	15%	9%	191%	14%
RMS Ratio (between the axes)		86%	Reduction		14%

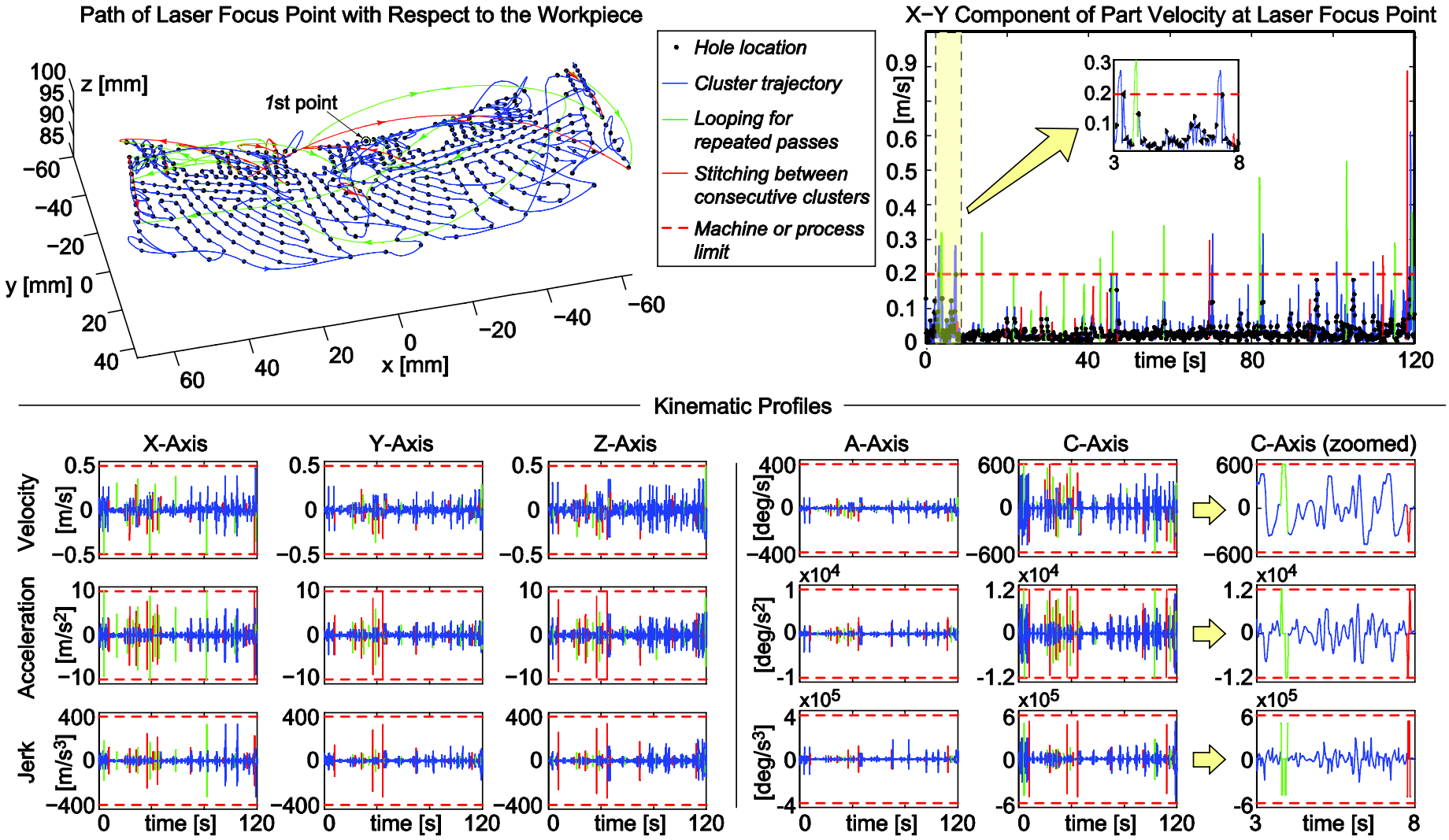

Figure 6.4: Implementation Results for a Gas Turbine Combustion Chamber Panel [Example #3]

Table 6.5: Cycle Time Comparison between the Optimized Spline Trajectory and Linear Interpolation with Full Stops through Consecutive Holes (assuming 1 laser shot per hole) [Example #3]

Cluster #	No. Of Points	Achievable Laser Frequency [Hz]	Used Laser Frequency [Hz]	Motion Duration [s]
1	31	9.7696	8.00	3.750
2	47	17.7263	8.00	5.750
3	14	15.3273	8.00	1.625
4	18	15.9436	8.00	2.125
5	10	17.9208	8.00	1.125
6	22	21.2392	8.00	2.625
7	17	18.1845	8.00	2.000
8	13	25.8700	8.00	1.500
9	10	11.5334	8.00	1.125
10	89	16.3960	8.00	11.000
11	98	12.7519	8.00	12.125
12	71	10.4779	8.00	8.750
13	13	11.4290	8.00	2.750
14	8	**8.5072**	8.00	0.875
Total:	**461**			**57.125**

Stitching Between Clusters	Motion Duration [s]
1→2	0.125
2→3	0.250
3→4	0.250
4→5	0.250
5→6	0.250
6→7	0.125

Total Duration for Clusters & Stitching [s]:
57.125 + 2.625 = **59.750**

Total Duration for Linear Interpolation (w/ full stops) [s]
63.625

7→8	0.250
8→9	0.125
9→10	0.250
10→11	0.125
11→12	0.250
12→13	0.125
13→14	0.250
Total:	**2.625**

[%] Time Reduction over Applying Linear Interpolation
6.09%

Table 6.6: Integral Square of Acceleration and Jerk Comparison between the Optimized Spline Trajectory and Linear Interpolation with Full Stops [Example #3]

Time Integral Square of Acceleration					
	X-Axis [mm^2/s^3]	Y-Axis [mm^2/s^3]	Z-Axis [mm^2/s^3]	A-Axis [deg^2/s^3]	C-Axis [deg^2/s^3]
Linear Interp.	8.68E+07	6.65E+07	1.86E+08	5.73E+06	2.37E+08
Spline Interp.	6.59E+07	3.57E+07	8.23E+07	7.61E+06	2.12E+08
Ratio (spline/linear)	76%	54%	44%	133%	89%
RMS Ratio (between the axes)		85%	Reduction		15%

Time Integral Square of Jerk					
	X-Axis [mm^2/s^5]	Y-Axis [mm^2/s^5]	Z-Axis [mm^2/s^5]	A-Axis [deg^2/s^5]	C-Axis [deg^2/s^5]
Linear Interp.	2.01E+11	1.68E+11	4.83E+11	1.36E+10	5.29E+11
Spline Interp.	6.16E+10	4.51E+10	7.64E+10	1.29E+10	2.32E+11
Ratio (spline/linear)	31%	27%	16%	95%	44%
RMS Ratio (between the axes)		51%	Reduction		49%

Chapter 7

Conclusions and Future Work

7.1 Conclusions

This thesis has presented a new and time-optimized trajectory generation technique for 5-axis on-the-fly laser drilling operations. Axis level velocity, acceleration, and jerk limits of the feed drives have been considered, along with a cap on the x-y component of part velocity at each hole location, in order to limit hole elongation. Time-optimized trajectories were generated for pre-sequenced hole clusters using the algorithm developed in Chapter 4, and the individual clusters were joined together or looped onto themselves using the stitching algorithm explained in Chapter 5. Both the cluster trajectory optimization, and looping/stitching algorithms guarantee a feasible solution and provide a substantial improvement (~56%) in the motion smoothness compared to using direct linear interpolation between the target hole locations. This helps reduce the vibrations induced onto the laser optics, which also enables higher processing speeds to be realized. There is also a modest reduction in the cycle time (~%6), due to the avoidance of unnecessary accelerations and decelerations between the hole locations. The overall trajectory optimization algorithm has been validated on three different sample aerospace parts with 567, 278 and 461 holes, which need to be drilled on-the-fly while all 5-axes are moving in coordination. The simulation results and preliminary experiments conducted on-site at Pratt & Whitney Canada have validated the success of the algorithm. Currently, further testing and integration is underway to incorporate this algorithm into the manufacturing process for gas turbine combustion chamber panels.

The solution sought in this thesis for on-the-fly laser drilling should be both easy and simple to implement, and also converge closely to an optimal solution, even if only local, with minimal restriction on the trajectory profile shape.

The open loop laser drilling technique relies on the ability of the machine axis encoders and closed loop positioning controllers to follow given trajectories within error tolerances. Each machine axis is controlled individually and the tracking errors need to be well within hole drilling procedure tolerances. Drilled parts are inspected after initial experiments and

tests are then approved for final drills and part duplications. Future work may incorporate a closed loop error tracking techniques to eliminate the uncertainty of propagating errors during the drilling process and increase the robustness of the used trajectory generation algorithm.

Current industrial machine tool controllers do not provide any specialized optimal trajectory generation algorithms that are suitable for 5-axis on-the-fly laser drilling. Furthermore, trajectory optimization techniques published in literature prior to this work have mainly focused on contour following applications or point-to-point motion (with variable intervals in between), and have not tackled the trajectory optimization problem for on-the-fly laser drilling. Hence, this thesis has clearly advanced the state-of-the-art in this field. As verified in simulation results, the resulting trajectories not only allow shorter motion cycles times to be achieved, by also reduce the integral square of jerk by typically 50-60%, thereby allowing the process speed to be pushed up even further without vibrating the laser optics.

7.2 Research Summary

The objective of this research was to generate optimized 5-axis acceleration continuous trajectories to produce on-the-fly laser drilled parts in minimal time, i.e. at maximum firing frequency. Hole cluster data is provided by the CAD/CAM software as different drilling zones. Each cluster should ideally be produced at a constant laser pulsing frequency. The constraints in this research are the axes velocity, acceleration, jerk limits and the X-Y component of part velocity at hole locations (to limit hole elongation).

Trajectory optimization for each cluster is achieved by formulating the time-optimal trajectory as quintic segments:

$$x = At^5 + Bt^4 + Ct^3 + Dt^2 + Et + F$$

and following four optimization steps:

1. Fitting a minimum-snap (i.e. *4*th derivative) quintic profile through the given points to obtain an initial sub-optimal guess:

$$Find \begin{Bmatrix} A, B, C, \\ D, E, F \end{Bmatrix} \; to\ Minimize \Rightarrow \int_0^{T_\Sigma} \left[\frac{d^4 x(t)}{dt^4} \right]^2 dt = \int_0^{T_\Sigma} \left[x^{(IV)}(t) \right]^2 dt$$

2. Applying appropriate time scaling to bring all profiles into their given limits.
3. Optimizing velocity and acceleration boundary conditions (*1*st and *2*nd derivative boundary conditions) at hole locations to allow for further time compression by finding the lower possible value of α, the time scaling factor:

$$\alpha = \left\{ \sum_{k=1}^{n} \left(\left| \frac{\dot{x}(k)}{\dot{x}_{\max}} \right|^{p} + \ldots + \left| \frac{\dot{c}(k)}{\dot{c}_{\max}} \right|^{p} + \left| \frac{v_{xy}(k)}{v_{xy,\max}} \right|^{p} \right) + \left[\sum_{k=1}^{n} \left(\left| \frac{\ddot{x}(k)}{\ddot{x}_{\max}} \right|^{p} + \ldots + \left| \frac{\ddot{c}(k)}{\ddot{c}_{\max}} \right|^{p} \right) \right]^{1/2} + \left[\sum_{k=1}^{n} \left(\left| \frac{\dddot{x}(k)}{\dddot{x}_{\max}} \right|^{p} + \ldots + \left| \frac{\dddot{c}(k)}{\dddot{c}_{\max}} \right|^{p} \right) \right]^{1/3} \right\}^{1/p}, \quad as \ p \to \infty$$

4. Applying the new time scaling indicated by α.

Looping and stitching of clusters is realized with nonzero position and velocity connections using jerk and acceleration limited time-optimal segments.

7.3 Future Work

The developed algorithm solves each cluster as a whole (by optimizing each cluster of holes as one complete set). Future work needs to focus on achieving the solution in moving windows, so that trajectories for clusters with larger numbers of holes can be efficiently broken down into smaller sub-clusters and optimized without requiring excessive off-line computation time.

In addition, the hole sequencing currently applied in the CAD/CAM software was found to be one of the major bottlenecks that limited the achievable laser pulsing frequency. New sequencing techniques need to be investigated, similar to the Traveling Salesman approach, which will work concurrently with the trajectory optimization algorithm developed in this study to yield further cycle time reduction compared to what was achieved with the pre-set hole sequence used in this thesis.

Incorporating dynamics will be necessary when incorporating algorithms that need to determine joint values (for rotary axes) and linear positions (for prismatic axes) and track position accuracies through closed loop controls after reading positions from the optimized trajectories.

Future optimization approaches will also include finding the optimal hole clusters (group of holes) to be drilled. This variable clustering of holes constrained by machine kinematics, coupled with finding the appropriate and optimized sequence of holes per cluster while considering other groups of holes, will be explored and is expected to provide further laser drilling cycle time reductions.

Furthermore, there is significant interest in the exploration of the theoretical globality of the solution. This is a very significant academic challenge, therefore, methods such as interval analysis, will be considered, which have been shown useful in finding global minimums.

7.4 Other Laser Drilling Applications

The high laser drilling peak power coupled with short pulse widths creates a perfect beam, which offers very good drilling capabilities in thin sheets, ceramics and silicon. The optics configuration can also be changed to achieve a different spot size, required for drilling various hole diameters. Thus, the high power drilling laser can be used for on-the-fly rock drilling applications, drilling of flow filters and strainers, sub-micron drilling in flexography ceramic rolls, high speed drilling of guide vanes, hole drilling of silicon, drilling diamonds for removing imperfections and on-the-fly drilling of cooling holes. The high peak and energy/pulse can also be used for drilling thick metals.

Appendix A:

5-Axis Laser Drilling Machine Kinematic Analysis

A.1 Kinematic Transformation

A diagram of the 5-axis kinematics is shown in Figure A.1.

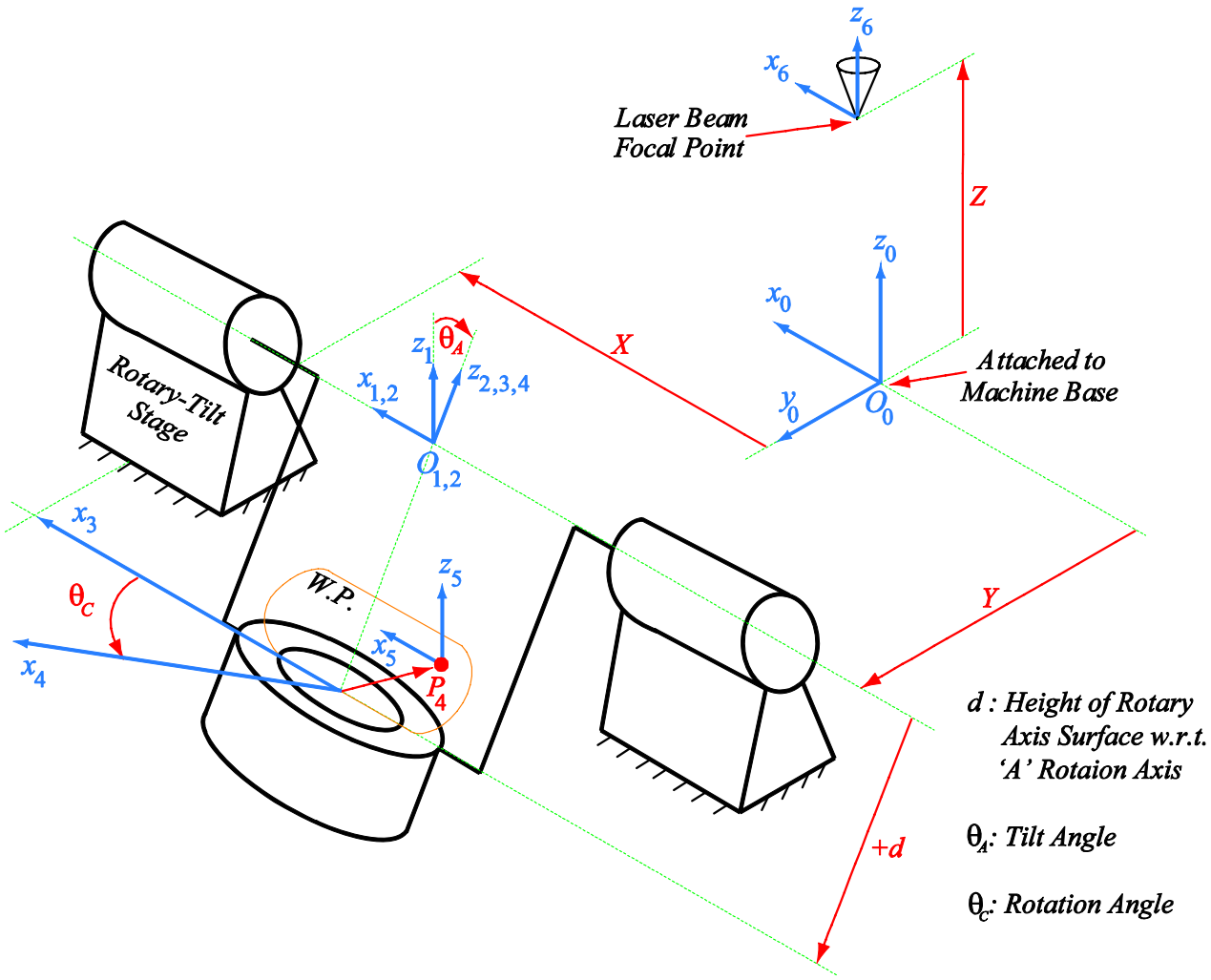

Figure A.1: 5-Axis Machine Coordinate Transfer Frames

The following coordinate systems (C.S's) are considered:

C.S.0 ($O_0 x_0 y_0 z_0$): This frame is fixed to the machine base, its axes are parallel to the translating joints of the machine.

C.S.1 ($O_1\ x_1\ y_1\ z_1$): Attached to the moving X-Y stage, x_1 and y_1 are parallel to the x_0 and y_0 axes. The center of frame (O_1) is located at mid-point of the tilt axis.

C.S.2 ($O_2\,x_2\,y_2\,z_2$): O_2 and z_2 are identical to O_1 and z_1. C.S.2 is obtained by rotating C.S.1 around its x-axis (x_1) by θ_A .

C.S.3 ($O_3\ x_3 y_3 z_3$): x_3 , y_3 and z_3 are identical to x_2 , y_2 , and z_2 . This frame is obtained by translating C.S.2 by "d" along its z-axis (z_2). The value for "d" can be negative or positive depending on the workpiece fixture being used.

C.S.4 ($O_4\ x_4 y_4 z_4$): O_4 and z_4 are identical to O_3 and z_3. This frame is obtained by rotating C.S.3 around its z-axis (z_3) by θ_C .

C.S.5 ($O_5\ x_5\ y_5 z_5$): This frame is parallel to C.S.4. Its origin (O_5) is translated to coincide with the hole being drilled on the workpiece.

C.S.6 ($O_6\ x_6\ y_6 z_6$): This frame is parallel to C.S.0 ($O_0 x_0 y_0 z_0$) and is fixed at the laser focal point.

Vector P_4: Position vector of current hole location on the workpiece defined in reference to C.S.4.

The transformation from C.S.1 to C.S.4 is as follows:

$$H_{14} = H_{12}H_{23}H_{34} = Rot_{x,\theta_A}\ Trans_{z,d}\ Rot_{z,\theta_C} \tag{A.1}$$

$$Rot: Rotational\ Matrix$$

$$Trans: Translational\ Matrix$$

Calculating each transformation matrix from O_0 to O_5 yields:

$$H_{05} = \underbrace{Trans_{x,y}}_{H_{01}}\ \underbrace{Rot_{x,\theta_A}}_{H_{12}}\ \underbrace{Trans_{z,d}}_{H_{23}}\ \underbrace{Rot_{z,\theta_C}}_{H_{34}}\ \underbrace{Trans_{P_4}}_{H_{45}} \tag{A.2}$$

In order to solve for the transformation matrix H_{05}, the in-between transformations H_{01}, H_{12} , H_{23} , H_{34} and H_{45} need to be calculated. In the following calculations $\{X, Y, Z\}$ represent X, Y and Z values read from the NC file. Also, $S_4 = \sin\theta_A$, $C_4 = \cos\theta_A$,

$S_5 = \sin\theta_C$, $C_5 = \cos\theta_C$ and $\{x_h, y_h, z_h\}$ represent hole coordinates (P_4) in C.S.4. Therefore,

$$H_{01} = \left[\begin{array}{ccc|c} & I_3 & & \begin{matrix}X\\Y\\0\end{matrix} \\ \hline 0 & 0 & 0 & 1 \end{array}\right] \quad H_{12} = \left[\begin{array}{ccc|c} 1 & 0 & 0 & 0 \\ 0 & C_4 & -S_4 & 0 \\ 0 & S_4 & C_4 & 0 \\ \hline 0 & 0 & 0 & 1 \end{array}\right] \quad H_{23} = \left[\begin{array}{ccc|c} & I_3 & & \begin{matrix}0\\0\\d\end{matrix} \\ \hline 0 & 0 & 0 & 1 \end{array}\right]$$

$$H_{34} = \left[\begin{array}{ccc|c} C_5 & -S_5 & 0 & 0 \\ S_5 & C_5 & 0 & 0 \\ 0 & 0 & 1 & 0 \\ \hline 0 & 0 & 0 & 1 \end{array}\right] \quad H_{45} = \left[\begin{array}{ccc|c} & I_3 & & \begin{matrix}x_h\\y_h\\z_h\end{matrix} \\ \hline 0 & 0 & 0 & 1 \end{array}\right]$$

Hence, H_{05} can be composed as:

$$H_{02} = H_{01}H_{12} = \left[\begin{array}{ccc|c} & I_3 & & \begin{matrix}X\\Y\\0\end{matrix} \\ \hline 0 & 0 & 0 & 1 \end{array}\right]\left[\begin{array}{ccc|c} 1 & 0 & 0 & 0 \\ 0 & C_4 & -S_4 & 0 \\ 0 & S_4 & C_4 & 0 \\ \hline 0 & 0 & 0 & 1 \end{array}\right] = \left[\begin{array}{ccc|c} 1 & 0 & 0 & X \\ 0 & C_4 & -S_4 & Y \\ 0 & S_4 & C_4 & 0 \\ \hline 0 & 0 & 0 & 1 \end{array}\right]$$

$$H_{03} = H_{02}H_{23} = \left[\begin{array}{ccc|c} 1 & 0 & 0 & X \\ 0 & C_4 & -S_4 & Y \\ 0 & S_4 & C_4 & 0 \\ \hline 0 & 0 & 0 & 1 \end{array}\right]\left[\begin{array}{ccc|c} 1 & 0 & 0 & 0 \\ 0 & 1 & 0 & 0 \\ 0 & 0 & 1 & d \\ \hline 0 & 0 & 0 & 1 \end{array}\right] = \left[\begin{array}{ccc|c} 1 & 0 & 0 & X \\ 0 & C_4 & -S_4 & Y - d\,S_4 \\ 0 & S_4 & C_4 & d\,C_4 \\ \hline 0 & 0 & 0 & 1 \end{array}\right]$$

$$H_{04} = H_{03}H_{34} = \left[\begin{array}{ccc|c} 1 & 0 & 0 & X \\ 0 & C_4 & -S_4 & Y - d\,S_4 \\ 0 & S_4 & C_4 & d\,C_4 \\ \hline 0 & 0 & 0 & 1 \end{array}\right]\left[\begin{array}{ccc|c} C_5 & -S_5 & 0 & 0 \\ S_5 & C_5 & 0 & 0 \\ 0 & 0 & 1 & 0 \\ \hline 0 & 0 & 0 & 1 \end{array}\right] = \left[\begin{array}{ccc|c} C_5 & -S_5 & 0 & X \\ C_4S_5 & C_4C_5 & -S_4 & Y - d\,S_4 \\ S_4S_5 & S_4C_5 & C_4 & d\,C_4 \\ \hline 0 & 0 & 0 & 1 \end{array}\right]$$

$$\therefore H_{05} = H_{04}H_{45} = \left[\begin{array}{ccc|c} C_5 & -S_5 & 0 & X \\ C_4S_5 & C_4C_5 & -S_4 & Y - d\,S_4 \\ S_4S_5 & S_4C_5 & C_4 & d\,C_4 \\ \hline 0 & 0 & 0 & 1 \end{array}\right]\left[\begin{array}{ccc|c} 1 & 0 & 0 & x_h \\ 0 & 1 & 0 & y_h \\ 0 & 0 & 1 & z_h \\ \hline 0 & 0 & 0 & 1 \end{array}\right] = \left[\begin{array}{ccc|c} C_5 & -S_5 & 0 & X_{05} \\ C_4S_5 & C_4C_5 & -S_4 & Y_{05} \\ S_4S_5 & S_4C_5 & C_4 & Z_{05} \\ \hline 0 & 0 & 0 & 1 \end{array}\right]$$

The position of the hole location (O_5) on the workpiece (X_{05}, Y_{05}, Z_{05}) with respect to the machine reference frame ($O_0\,x_0\,y_0\,z_0$) can be calculated with the following equations:

$$X_{05} = X + x_h C_5 - y_h S_5$$

$$Y_{05} = Y - d\,S_4 + x_h C_4 S_5 + y_h C_4 C_5 - z_h S_4$$

$$Y_{05} = Y + C_4(x_h S_5 + y_h C_5) - S_4(d + z_h)$$

$$Z_{05} = x_h S_4 S_5 + y_h S_4 C_5 + z_h C_4 + d\,C_4$$

$$= S_4(x_h S_5 + y_h C_5) + C_4(z_h + d)$$

Remembering that $C_4 = \cos\theta_A$, $S_4 = \sin\theta_A$, $C_5 = \cos\theta_C$, $S_5 = \sin\theta_C$,

$$X_{05} = X + x_h \cos\theta_C - y_h \sin\theta_C$$

$$Y_{05} = Y + \cos\theta_A(x_h \sin\theta_C + y_h \cos\theta_C) - \sin\theta_A(d + z_h) \tag{A.3}$$

$$Z_{05} = \sin\theta_A(x_h \sin\theta_C + y_h \cos\theta_C) + \cos\theta_A(z_h + d)$$

The z-axis motion with respect to machine base can be expressed as:

$$H_{06} = Trans_z = \left[\begin{array}{ccc:c} & I_3 & & \begin{matrix}0\\0\\Z\end{matrix} \\ \hdashline 0 & 0 & 0 & 1 \end{array}\right]$$

Hence, the hole motion with respect to laser head focal point can be obtained as:

$$H_{65} = H_{60}H_{05} = (H_{06})^{-1} H_{05}$$

$$H_{65} = \left[\begin{array}{ccc:c} 1 & 0 & 0 & 0 \\ 0 & 1 & 0 & 0 \\ 0 & 0 & 1 & -Z \\ \hdashline 0 & 0 & 0 & 1 \end{array}\right]\left[\begin{array}{ccc:c} C_5 & -S_5 & 0 & X_{05} \\ C_4S_5 & C_4C_5 & -S_4 & Y_{05} \\ S_4S_5 & S_4C_5 & C_4 & Z_{05} \\ \hdashline 0 & 0 & 0 & 1 \end{array}\right] = \left[\begin{array}{ccc:c} C_5 & -S_5 & 0 & X_{05} \\ C_4S_5 & C_4C_5 & -S_4 & Y_{05} \\ S_4S_5 & S_4C_5 & C_4 & Z_{05} - Z \\ \hdashline 0 & 0 & 0 & 1 \end{array}\right]$$

$$\therefore \quad \begin{aligned} X_{65} &= X_{05} \\ Y_{65} &= Y_{05} \\ Z_{65} &= Z_{05} - Z \end{aligned} \tag{A.4}$$

A.2 Reconstruction of Hole Position Data from NC Code

With the knowledge that every hole is to be drilled at the laser focus point ($X_{65}=0$, $Y_{65}=0$, $Z_{65}=0$), it is possible to re-construct the position of each hole $P_4=(x_h, y_h, z_h)$ in the workpiece coordinate system, using hole data contained in the NC (Numerical Control) file:

$$\begin{aligned} X_{65} &= X + x_h\cos\theta_C - y_h\sin\theta_C = 0 \\ Y_{65} &= Y + \cos\theta_A(x_h\sin\theta_C + y_h\cos\theta_C) - \sin\theta_A(d+z_h) = 0 \\ Z_{65} &= \sin\theta_A(x_h\sin\theta_C + y_h\cos\theta_C) + \cos\theta_A(z_h+d) - Z = 0 \end{aligned} \tag{A.5}$$

Isolating unknown variables:

$$\left[\begin{array}{c|c|c} \cos\theta_C & -\sin\theta_C & 0 \\ \cos\theta_A\sin\theta_C & \cos\theta_A\cos\theta_C & -\sin\theta_A \\ \sin\theta_A\sin\theta_C & \sin\theta_A\cos\theta_C & \cos\theta_A \end{array}\right] \bullet \begin{bmatrix} x_h \\ y_h \\ d+z_h \end{bmatrix} = \begin{bmatrix} -X \\ -Y \\ Z \end{bmatrix}$$

$$\underbrace{\left[\begin{array}{c|c|c} C_5 & -S_5 & 0 \\ C_4S_5 & C_4C_5 & -S_4 \\ S_4S_5 & S_4C_5 & C_4 \end{array}\right]}_{R_{65}=R_{05}} \bullet \underbrace{\begin{bmatrix} x_h \\ y_h \\ d+z_h \end{bmatrix}}_{Unknown} = \underbrace{\begin{bmatrix} -X \\ -Y \\ Z \end{bmatrix}}_{Known} \tag{A.6}$$

Noting that $R_{05}^{-1}=R_{05}^{T}$ (property of rotation matrices), also noting that $R_{05}(\theta_A, \theta_C)$, the unknowns can be calculated as:

$$\therefore \begin{bmatrix} x_h \\ y_h \\ d+z_h \end{bmatrix} = R_{05}^{T} \begin{bmatrix} -X \\ -Y \\ l+Z \end{bmatrix} \tag{A.7}$$

A sample implementation of this solution is shown in Figure A.2 and Figure A.3. Figure A.2 shows the x-y-z axes coordinates programmed in the NC code for the machine's axes and Figure A.3 show the re-constructed hole locations on the workpiece, by applying the transformation in Eq. (A.7). This transformation has also been used for visualizing the path of the laser focal point on the workpiece coordinates (C.S.4).

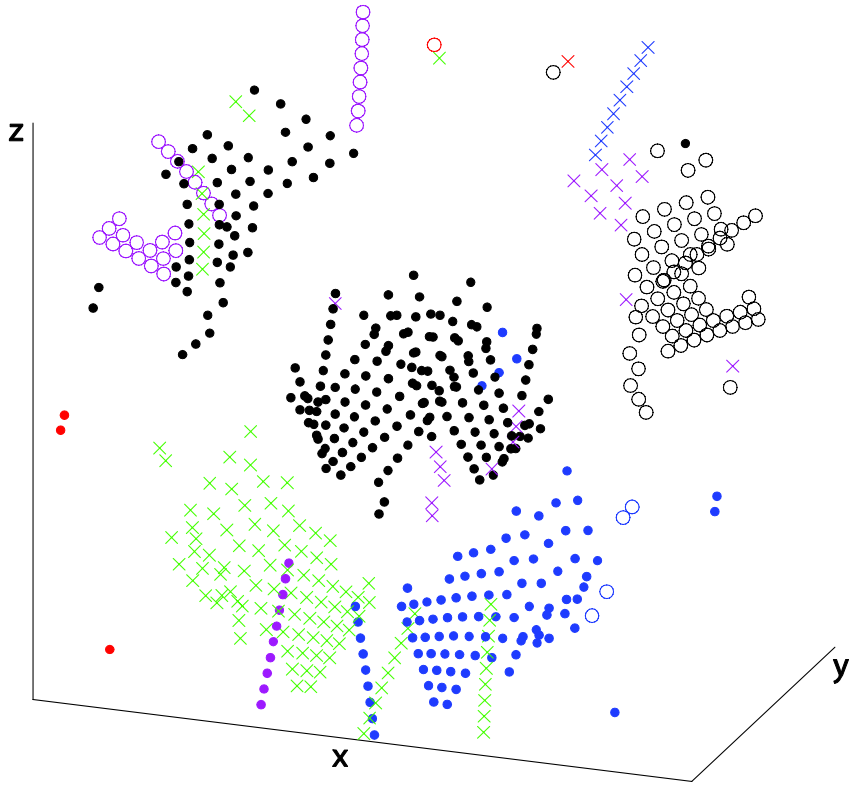

Figure A.2: NC File X, Y, Z Data Denoting Hole Locations

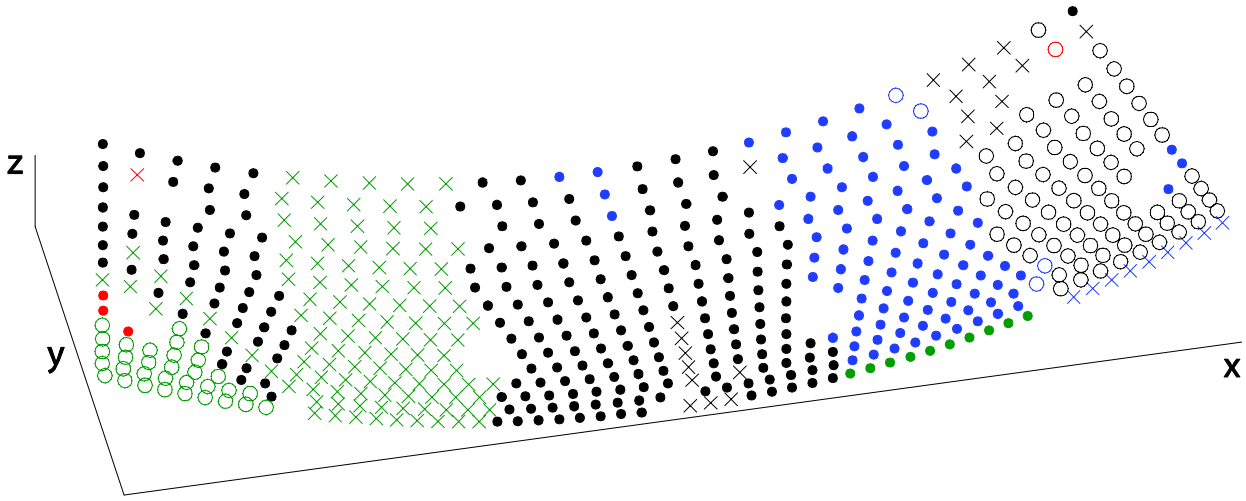

Figure A.3: Workpiece Hole Locations in C.S.4

A.3 Part Velocity Component at Hole Location Orthogonal to the Laser Beam

After successfully calculating the hole locations x_h, y_h and z_h with respect to C.S.4, it is possible to calculate the part velocity with respect to the laser focal point at hole locations.

By differentiating Eq. (A.5) with respect to time, we obtain:

$$\dot{x}_{65} = \dot{X} - x_h \sin\theta_C \bullet \dot{\theta}_C - y_h \cos\theta_C \bullet \dot{\theta}_C$$

$$\dot{x}_{65} = \underbrace{1}_{*}\ \dot{X} - \underbrace{\left(x_h \sin\theta_C - y_h \cos\theta_C\right)}_{**} \bullet \dot{\theta}_C \tag{A.8}$$

Note that $*$ and $**$, in Eq. (A.8) represent terms in the 5-axis machine Jacobian matrix.

Similarly for the y-axis:

$$\begin{aligned}\dot{y}_{65} = \dot{Y} &+ \cos\theta_A \bullet \dot{\theta}_C \bullet \left(x_h \cos\theta_C - y_h \sin\theta_C\right) \\ &- \sin\theta_A \bullet \dot{\theta}_A \bullet \left(x_h \sin\theta_C + y_h \cos\theta_C\right) \\ &- \cos\theta_A \bullet \dot{\theta}_A \bullet \left(d + z_h\right)\end{aligned}$$

$$\begin{aligned}\dot{y}_{65} = \dot{Y} &+ \cos\theta_A \bullet \dot{\theta}_C \bullet \left(x_h \cos\theta_C - y_h \sin\theta_C\right) \\ &- \dot{\theta}_A \bullet \left[\sin\theta_A \left(x_h \sin\theta_C + y_h \cos\theta_C\right) + \cos\theta_A \left(d + z_h\right)\right]\end{aligned} \tag{A.9}$$

and for z-axis:

$$\begin{aligned}\dot{z}_{65} = -\dot{Z} &+ \sin\theta_A \bullet \dot{\theta}_C \bullet \left(x_h \cos\theta_C - y_h \sin\theta_C\right) \\ &+ \dot{\theta}_A \bullet \left[\cos\theta_A \left(x_h \sin\theta_C + y_h \cos\theta_C\right) - \sin\theta_A \left(d + z_h\right)\right]\end{aligned} \tag{A.10}$$

The X-Y plane velocity governing hole elongation during drilling the operation can be obtained as:

$$V_{xy} = \sqrt{\dot{x}_{65}^2 + \dot{y}_{65}^2} \tag{A.11}$$

Appendix B:

Minimum-Snap Quintic Spline Trajectory Generation

The detailed mathematical derivation to achieve a minimum-snap trajectory is provided. Due to the flexibility and ease of parameterization, and for acceleration continuity, a quintic spline has been chosen as the basis curve. Subsequently, the laser position, velocity, acceleration, jerk and snap profiles for the *k*th segment in the x-axis are expressed in Eq. (B.1):

$$\begin{aligned} x_k(t) &= A_k t^5 + B_k t^4 + C_k t^3 + D_k t^2 + E_k t + F_k \\ \dot{x}_k(t) &= 5A_k t^4 + 4B_k t^3 + 3C_k t^2 + 2D_k t + E_k \\ \ddot{x}_k(t) &= 20A_k t^3 + 12B_k t^2 + 6C_k t + 2D_k \qquad , \quad 0 \le t \le T_k \\ \dddot{x}_k(t) &= 60A_k t^2 + 24B_k t + 6C_k \\ \ddddot{x}_k(t) &= x_k^{IV}(t) = 120A_k t + 24B_k \end{aligned} \tag{B.1}$$

Above, T_k is the segment duration. The objective function for minimizing the integral square of snap for the *k*th segment is given in Eq. (B.2):

$$S_k = \frac{1}{2}\int_0^{T_k}\left(\frac{d^4 x_k(t)}{dt^4}\right)^2 dt = \frac{1}{2}\int_0^{T_k}(120A_k t + 24B_k)^2\, dt = \frac{1}{2}\left(4800T_k^3 + 2880A_k B_k T_k^2 + 576B_k^2 T_k\right)$$

$$= \frac{1}{2}\underbrace{\begin{bmatrix} A_k & B_k & C_k & D_k & E_k & F_k \end{bmatrix}}_{\boldsymbol{\theta}_k^T}\underbrace{\begin{bmatrix} 4800T_k^3 & 1440T_k^2 & 0_{1\times4} \\ 1440T_k^2 & 576T_k & 0_{1\times4} \\ 0_{4\times1} & 0_{4\times1} & 0_{4\times4} \end{bmatrix}}_{\mathbf{K}_k}\underbrace{\begin{bmatrix} A_k \\ B_k \\ C_k \\ D_k \\ E_k \\ F_k \end{bmatrix}}_{\boldsymbol{\theta}_k} = \frac{1}{2}\boldsymbol{\theta}_k^T \mathbf{K}_k \boldsymbol{\theta}_k \tag{B.2}$$

Above, the vector $\boldsymbol{\theta}_k = \begin{bmatrix} A_k & B_k & C_k & D_k & E_k & F_k \end{bmatrix}^{\mathrm{T}}$ contains the parameters (segment quintic equation coefficients) of the *k*th segment. Considering that within a cluster, all segments will have the same duration which is equal to the laser pulsing period (i.e.

$T_1 = T_2 = \ldots = T_N = T$), the minimum-snap objective function for a cluster of N segments can be expressed as,

$$S = \sum_{k=1}^{N} S_k = \frac{1}{2} \underbrace{\begin{bmatrix} \boldsymbol{\theta}_1^T & \boldsymbol{\theta}_2^T & \ldots & \boldsymbol{\theta}_N^T \end{bmatrix}}_{\boldsymbol{\theta}^T} \underbrace{\begin{bmatrix} \mathbf{K}_1(T) & & & 0 \\ & \mathbf{K}_2(T) & & \\ & & \ddots & \\ 0 & & & \mathbf{K}_N(T) \end{bmatrix}}_{\mathbf{K}} \underbrace{\begin{bmatrix} \boldsymbol{\theta}_1 \\ \boldsymbol{\theta}_2 \\ \vdots \\ \boldsymbol{\theta}_N \end{bmatrix}}_{\boldsymbol{\theta}} = \frac{1}{2} \boldsymbol{\theta}^T \mathbf{K}(T) \boldsymbol{\theta} \tag{B.3}$$

The position profile has to pass through the hole locations $\{ X_1, X_2, ..., X_{N+1} \}$ at instances designated by the segment durations. For the *k*th segment, the following position boundary conditions need to hold:

$$x_k(0) = X_k \quad , \quad x_k(T) = X_{k+1} \tag{B.4}$$

Using Eq. (B.1), this can be written in matrix from as,

$$\underbrace{\begin{bmatrix} 0 & 0 & 0 & 0 & 0 & 1 \\ T^5 & T^4 & T^3 & T^2 & T & 1 \end{bmatrix}}_{\boldsymbol{L}_k^0(T)} \begin{bmatrix} A_k \\ B_k \\ C_k \\ D_k \\ E_k \\ F_k \end{bmatrix} = \underbrace{\begin{bmatrix} X_k \\ X_{k+1} \end{bmatrix}}_{\boldsymbol{\xi}_k^0} \Rightarrow \boldsymbol{L}_k^0(T) \boldsymbol{\theta}_k = \boldsymbol{\xi}_k^0 \tag{B.5}$$

The knot position constraints from all segments can be grouped together as,

$$\underbrace{\begin{bmatrix} \boldsymbol{L}_1^0(T) & 0_{2\times 6} & & 0 \\ 0_{2\times 6} & \boldsymbol{L}_2^0(T) & & \\ & & \ddots & \\ 0 & & & \boldsymbol{L}_N^0(T) \end{bmatrix}}_{\boldsymbol{L}^0(T)} \begin{bmatrix} \boldsymbol{\theta}_1 \\ \boldsymbol{\theta}_2 \\ \vdots \\ \boldsymbol{\theta}_N \end{bmatrix} = \underbrace{\begin{bmatrix} \boldsymbol{\xi}_1^0 \\ \boldsymbol{\xi}_2^0 \\ \vdots \\ \boldsymbol{\xi}_N^0 \end{bmatrix}}_{\boldsymbol{\xi}^0} \Rightarrow \boldsymbol{L}^0(T) \boldsymbol{\theta} = \boldsymbol{\xi}^0 \tag{B.6}$$

The velocity, acceleration, and jerk continuity constraints at the knot joining the *k*th and *k+1*st segments can be written as:

$$\left.\begin{aligned} \dot{x}_k(T) &= \dot{x}_{k+1}(0) \\ \ddot{x}_k(T) &= \ddot{x}_{k+1}(0) \\ \dddot{x}_k(T) &= \dddot{x}_{k+1}(0) \end{aligned}\right\} \Rightarrow \left\{\begin{aligned} \dot{x}_k(T) - \dot{x}_{k+1}(0) &= 0 \\ \ddot{x}_k(T) - \ddot{x}_{k+1}(0) &= 0 \\ \dddot{x}_k(T) - \dddot{x}_{k+1}(0) &= 0 \end{aligned}\right\} \tag{B.7}$$

Substituting the expressions for $\dot{x}_k(t)$, $\ddot{x}_k(t)$, and $\dddot{x}_k(t)$ from Eq. (B.1) into (B.7) results in,

$$\underbrace{\left[\begin{array}{cccccc|cccccc} 5T^4 & 4T^3 & 3T^2 & 2T & 1 & 0 & 0 & 0 & 0 & 0 & -1 & 0 \\ 20T^3 & 12T^2 & 6T & 2 & 0 & 0 & 0 & 0 & 0 & -2 & 0 & 0 \\ 60T^2 & 24T & 6 & 0 & 0 & 0 & 0 & 0 & -6 & 0 & 0 & 0 \end{array}\right]}_{\mathcal{L}_{k,k+1}^{123}(T)} \cdot \begin{bmatrix} \theta_k \\ \theta_{k+1} \end{bmatrix} = \begin{bmatrix} 0 \\ 0 \\ 0 \end{bmatrix} \tag{B.8}$$

The derivative continuity conditions can be grouped together as,

$$\underbrace{\begin{bmatrix} \mathbf{L}_{1,2}^{123}(T) & 0_{3\times 6} & & 0 \\ 0_{3\times 6} & \mathbf{L}_{2,3}^{123}(T) & & \\ & \ddots & & \\ 0 & & & \mathbf{L}_{N-1,N}^{123}(T) \end{bmatrix}}_{\mathbf{L}^{123}} \begin{bmatrix} \boldsymbol{\theta}_1 \\ \boldsymbol{\theta}_2 \\ \vdots \\ \boldsymbol{\theta}_N \end{bmatrix} = \underbrace{0_{3(N-1)\times 1}}_{\boldsymbol{\xi}^{123}} \Rightarrow \mathbf{L}^{123}(T)\boldsymbol{\theta} = \boldsymbol{\xi}^{123} \tag{B.9}$$

If initial conditions of velocity ($\dot{X}_0$), acceleration ($\ddot{X}_0$), and jerk ($\dddot{X}_0$) are provided at the beginning of the first segment, they can be included into the formulation as $\dot{x}_1(0) = \dot{X}_0$, $\ddot{x}_1(0) = \ddot{X}_0$, and $\dddot{x}_1(0) = \dddot{X}_0$. This can be expressed in matrix form using Eq. (B.1):

$$\underbrace{\left[\begin{array}{cccccc|c} 0 & 0 & 0 & 0 & 1 & 0 & \\ 0 & 0 & 0 & 2 & 0 & 0 & 0_{3\times 6(N-1)} \\ 0 & 0 & 6 & 0 & 0 & 0 & \end{array}\right]}_{\boldsymbol{L}^{init}} \begin{bmatrix} \boldsymbol{\theta}_1 \\ \boldsymbol{\theta}_2 \\ \vdots \\ \boldsymbol{\theta}_N \end{bmatrix} = \underbrace{\begin{bmatrix} \dot{X}_0 \\ \ddot{X}_0 \\ \dddot{X}_0 \end{bmatrix}}_{\boldsymbol{\xi}^{init}} \Rightarrow \boldsymbol{L}^{init}\boldsymbol{\theta} = \boldsymbol{\xi}^{init} \tag{B.10}$$

Similarly, if final conditions of velocity ($\dot{X}_f$), acceleration ($\ddot{X}_f$), and jerk ($\dddot{X}_f$) are provided at the end of the last segment, they can be included into the formulation as $\dot{x}_N(T) = \dot{X}_f$, $\ddot{x}_N(T) = \ddot{X}_f$, and $\dddot{x}_N(T) = \dddot{X}_f$. In matrix form, using Eq. (B.1), this becomes:

$$\underbrace{\left[\begin{array}{c|cccccc} & 5T^4 & 4T^3 & 3T^2 & 2T & 1 & 0 \\ 0_{3\times 6(N-1)} & 20T^3 & 12T^2 & 6T & 2 & 0 & 0 \\ & 60T^2 & 24T & 6 & 0 & 0 & 0 \end{array}\right]}_{\boldsymbol{L}^{final}} \begin{bmatrix} \boldsymbol{\theta}_1 \\ \boldsymbol{\theta}_2 \\ \vdots \\ \boldsymbol{\theta}_N \end{bmatrix} = \underbrace{\begin{bmatrix} \dot{X}_0 \\ \ddot{X}_0 \\ \dddot{X}_0 \end{bmatrix}}_{\boldsymbol{\xi}^{final}} \Rightarrow \boldsymbol{L}^{final}\boldsymbol{\theta} = \boldsymbol{\xi}^{final} \tag{B.11}$$

The knot position, *1*st, *2*nd, and *3*rd derivative continuity, and initial and final boundary condition constraints obtained in Eqs. (B.6), (B.9), (B.10), and (B.11) are stacked together in the form:

$$\underbrace{\begin{bmatrix} L^0(T) \\ L^{123}(T) \\ L^{init} \\ L^{final}(T) \end{bmatrix}}_{\boldsymbol{L}(T)} \boldsymbol{\theta} = \underbrace{\begin{bmatrix} \xi^0 \\ \xi^{123} \\ \xi^{init} \\ \xi^{final} \end{bmatrix}}_{\xi} \Rightarrow \boldsymbol{L}(T)\boldsymbol{\theta} = \boldsymbol{\xi} \tag{B.12}$$

The minimum-snap trajectory optimization problem subject to the constraints in Eq. (B.12) can be written as,

$$\left.\begin{aligned} \min_{\boldsymbol{\theta}} \quad & \frac{1}{2}\boldsymbol{\theta}^T \boldsymbol{K}(T)\boldsymbol{\theta} \\ \text{subject to:} \quad & \boldsymbol{L}(T)\boldsymbol{\theta} - \boldsymbol{\xi} = 0 \end{aligned}\right\} \tag{B.13}$$

Introducing the vector of Lagrange multipliers, $\boldsymbol{\Lambda} = [\Lambda_1, \Lambda_2, \ldots, \Lambda_{5N+3}]^T$, the augmented objective function can be written as,

$$S'(\boldsymbol{\theta}, \boldsymbol{\Lambda}) = \frac{1}{2}\boldsymbol{\theta}^T \boldsymbol{K}(T)\boldsymbol{\theta} + \boldsymbol{\Lambda}^T (\boldsymbol{L}(T)\boldsymbol{\theta} - \boldsymbol{\xi}) \tag{B.14}$$

Equating the partial derivates to zero ($\partial S'/\partial \boldsymbol{\theta} = 0$ and $\partial S'/\partial \boldsymbol{\Lambda} = 0$) yields the linear equation system,

$$\left.\begin{aligned} & \boldsymbol{K}(T)\boldsymbol{\theta} + \boldsymbol{L}^T(T)\boldsymbol{\Lambda} = 0 \\ & \boldsymbol{L}(T)\boldsymbol{\theta} = \boldsymbol{\xi} \end{aligned}\right\} \Rightarrow \begin{bmatrix} \boldsymbol{K}(T) & \boldsymbol{L}^T(T) \\ \boldsymbol{L}(T) & \boldsymbol{0} \end{bmatrix} \cdot \begin{bmatrix} \boldsymbol{\theta} \\ \boldsymbol{\Lambda} \end{bmatrix} = \begin{bmatrix} 0 \\ \boldsymbol{\xi} \end{bmatrix} \tag{B.15}$$

which has full rank as long as the segment duration is nonzero. Solution of the above linear equation system yields the coefficients $\boldsymbol{\theta}$ of the minimum-snap profile complying with all of the imposed constraints. Following the solution of Eq. (B.15), the position, velocity, acceleration, and jerk profiles can be generated using Eq. (B.1).

Other Profile-Optimized Trajectory Fittings: The mathematical derivation for the minimum-snap trajectory can also be applied for minimizing other similar objective functions. A different objective function that includes the integral square of normalized jerk, acceleration and velocity can expressed in the form:

$$
\begin{aligned}
\textit{Objective Function} &= \int_0^T \left(\frac{\dddot{x}(t)}{J_{\max}} \right)^2 dt + \int_0^T \left(\frac{\ddot{x}(t)}{A_{\max}} \right)^2 dt + \int_0^T \left(\frac{\dot{x}(t)}{V_{\max}} \right)^2 dt \\
&= \frac{1}{J_{\max}^2} \int_0^T \left(\dddot{x}(t) \right)^2 dt + \frac{1}{A_{\max}^2} \int_0^T \left(\ddot{x}(t) \right)^2 dt + \frac{1}{V_{\max}^2} \int_0^T \left(\dot{x}(t) \right)^2 dt \\
&= \frac{1}{J_{\max}^2} \theta^T K_j \theta + \frac{1}{A_{\max}^2} \theta^T K_a \theta + \frac{1}{V_{\max}^2} \theta^T K_v \theta \\
&= \theta^T \underbrace{\left[\frac{1}{J_{\max}^2} K_j + \frac{1}{A_{\max}^2} K_a + \frac{1}{V_{\max}^2} K_v \right]}_{K(T)} \theta
\end{aligned}
\tag{B.16}
$$

By expanding the $\left(\dddot{x}(t) \right)^2$, $\left(\ddot{x}(t) \right)^2$, $\left(\dot{x}(t) \right)^2$ terms in Eq. (B.16) and performing the integrals, K_j, K_a, K_v can be found as:

$$
K_j = \begin{bmatrix}
720T^5 & 360T^4 & 120T^3 & 0_{1\times3} \\
360T^4 & 192T^3 & 72T^2 & 0_{1\times3} \\
120T^3 & 72T^2 & 36T & 0_{1\times3} \\
0_{3\times1} & 0_{3\times1} & 0_{3\times1} & 0_{3\times3}
\end{bmatrix}
\tag{B.17}
$$

$$
K_a = \begin{bmatrix}
\left(400/7\right)T^7 & 40T^6 & 24T^5 & 10T^4 & 0_{1\times2} \\
40T^6 & \left(144/5\right)T^5 & 18T^4 & 8T^3 & 0_{1\times2} \\
24T^5 & 18T^4 & 12T^3 & 6T^2 & 0_{1\times2} \\
10T^4 & 8T^3 & 6T^2 & 4T & 0_{1\times2} \\
0_{2\times1} & 0_{2\times1} & 0_{2\times1} & 0_{2\times1} & 0_{2\times2}
\end{bmatrix}
\tag{B.18}
$$

$$
K_v = \begin{bmatrix}
\left(25/9\right)T^9 & \left(5/2\right)T^8 & \left(15/7\right)T^7 & \left(5/3\right)T^6 & T^5 & 0 \\
\left(5/2\right)T^8 & \left(16/7\right)T^7 & 2T^6 & \left(8/5\right)T^5 & T^4 & 0 \\
\left(15/7\right)T^7 & 2T^6 & \left(9/5\right)T^5 & \left(3/2\right)T^4 & T^3 & 0 \\
\left(5/3\right)T^6 & \left(8/5\right)T^5 & \left(3/2\right)T^4 & \left(4/3\right)T^3 & T^2 & 0 \\
T^5 & T^4 & T^3 & T^2 & T & 0 \\
0 & 0 & 0 & 0 & 0 & 0
\end{bmatrix}
\tag{B.19}
$$

Appendix C:

Effect of Uniform Time Scaling on the Derivative Profile

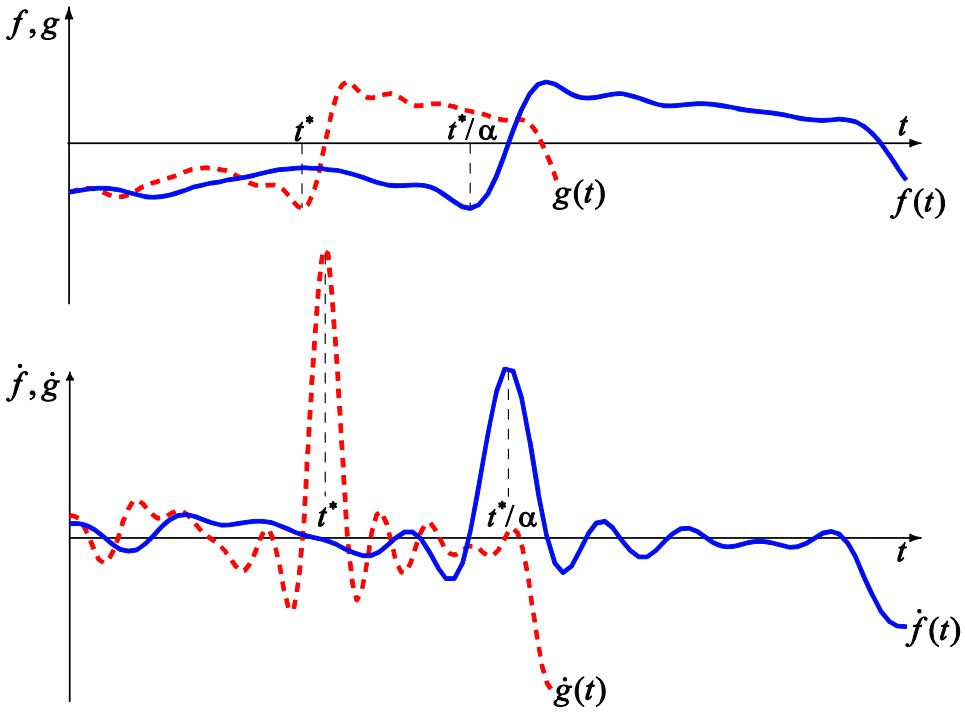

Figure C.1: Effect of Time Scaling a Function on its Derivative Profile

Considering that the position profile can be expressed as a function of time (i.e., $x = f(t)$), scaling the time variable by α will modify the position profile to become $g(t) = f(t/\alpha)$. In the following, it is analytically verified that this will also scale the velocity, acceleration, and jerk profiles by $1/\alpha$, $1/\alpha^2$, and $1/\alpha^3$:

$$\dot{g}(t) = \frac{1}{\alpha}\dot{f}(t/\alpha)\,,\ \ddot{g}(t) = \frac{1}{\alpha^2}\ddot{f}(t/\alpha)\,,\ \dddot{g}(t) = \frac{1}{\alpha^3}\dddot{f}(t/\alpha) \tag{C.1}$$

Given a function $f(t)$, as shown in Figure C.1, define an input (time) scaled function:

$$g(t) = f(t/\alpha) \tag{C.2}$$

for the scaling factor $\alpha > 0$. At a particular value of time: $t = t^*$, it can be shown that: $g(t^*) = f(t^*/\alpha)$. The objective is to find:

$$\left.\frac{dg(t)}{dt}\right|_{t=t^*} = \dot{g}(t^*) \tag{C.3}$$

Defining $\tau = \frac{t}{\alpha}$, then $\frac{d\tau}{dt} = \frac{1}{\alpha}$ and for $t = t^* \Rightarrow \tau = \tau^* = \frac{t^*}{\alpha}$. Hence, the effect of time scaling on the velocity profile can be obtained as:

$$\left.\frac{dg}{dt}\right|_{t=t^*} = \left.\frac{df\left(\frac{t}{\alpha}\right)}{dt}\right|_{t=t^*} = \left.\underbrace{\frac{df(\tau)}{d\tau}}_{=\left.\frac{df(t)}{dt}\right|_{t=\tau}} \cdot \underbrace{\frac{d\tau}{dt}}_{\frac{1}{\alpha}}\right|_{\tau=\tau^*=t^*/\alpha} = \frac{1}{\alpha}\left.\frac{df}{dt}\right|_{t=t^*/\alpha} = \frac{1}{\alpha}\dot{f}(t^*/\alpha)$$

Hence, for a particular value of time $t = t^*$,

$$\dot{g}(t^*) = \frac{1}{\alpha}\dot{f}(t^*/\alpha) \tag{C.4}$$

For any value of time ($t^* = t$), verifying the velocity scaling identity in Eq. (C.1), we have:

$$\boxed{\dot{g}(t) = \frac{1}{\alpha}\dot{f}(t/\alpha)} \quad \leftarrow \text{Velocity scaling by } \frac{1}{\alpha} \tag{C.5}$$

Similarly, $\ddot{g}(t)$ and $\dddot{g}(t)$ can be investigated as follows:

$$\left.\frac{d\dot{g}}{dt}\right|_{t=t^*} = \left.\frac{d}{dt}\left[\frac{1}{\alpha}\dot{f}\left(\frac{t}{\alpha}\right)\right]\right|_{t=t^*} = \frac{1}{\alpha}\cdot\underbrace{\frac{d\dot{f}\left(\frac{t}{\alpha}\right)}{d\left(\frac{t}{\alpha}\right)}}_{\tau}\cdot\left.\underbrace{\frac{d\left(\frac{t}{\alpha}\right)}{dt}}_{\frac{1}{\alpha}}\right|_{\tau=\tau^*=\frac{t^*}{\alpha}}$$

$$= \frac{1}{\alpha}\underbrace{\frac{d\dot{f}(\tau)}{d\tau}}_{\left.\frac{d\dot{f}}{dt}\right|_{t=\tau}}\cdot\frac{1}{\alpha}\Bigg|_{\tau=\tau^*=\frac{t^*}{\alpha}} = \frac{1}{\alpha^2}\ddot{f}(t^*/\alpha)$$

Therefore,

$$\ddot{g}(t^*) = \frac{1}{\alpha^2}\ddot{f}(t^*/\alpha) \quad \Rightarrow \quad \boxed{\ddot{g}(t) = \frac{1}{\alpha^2}\ddot{f}(t/\alpha)} \quad \leftarrow \text{Acceleration scaling by } \frac{1}{\alpha^2} \tag{C.6}$$

And, for the jerk profile:

$$\left.\frac{d}{dt}\dddot{g}\right|_{t=t^*} = \frac{d}{dt}\left[\frac{1}{\alpha^2}\ddot{f}\left(\frac{t}{\alpha}\right)\right]\Bigg|_{t=t^*} = \frac{1}{\alpha^2}\cdot\underbrace{\frac{d\ddot{f}\left(\overbrace{\frac{t}{\alpha}}^{\tau}\right)}{d\left(\frac{t}{\alpha}\right)}}_{\left.\frac{d\ddot{f}(t)}{dt}\right|_{t=\tau}}\cdot\overbrace{\frac{d\tau}{dt}}^{\frac{1}{\alpha}}\Bigg|_{\tau=\tau^*=\frac{t^*}{\alpha}} \tag{C.7}$$

Therefore,

$$\dddot{g}(t^*) = \frac{1}{\alpha^3}\dddot{f}(t^*/\alpha) \quad \Rightarrow \quad \boxed{\dddot{g}(t) = \frac{1}{\alpha^3}\dddot{f}(t/\alpha)} \quad \leftarrow \text{Jerk scaling by } \frac{1}{\alpha^3} \tag{C.8}$$

References

[1] Elfizy A., High Speed Laser Drilling Machine and Method, US Patent No US7,538,296 B2, May 26, 2009.

[2] Bobrow, J. E., Dubowsky, S., Gibson, J. S., 1985, "Time-optimal Control of Robotic Manipulators Along Specified Paths", International Journal of Robotics Research, Vol. 4, No. 3, pp. 3-17.

[3] Altintas, Y., Erkorkmaz, K., 2003. "Feedrate Optimization for Spline Interpolation in High Speed Machine Tools", Annals of CIRP, Vol. 49, No. 1, pp. 265-270.

[4] Huang T, Wang PF, Mei JP, Zhao XM, Chetwynd DG (2007) Time Minimum Trajectory Planning of a 2-DOF Translational Parallel Robot for Pick-and-Place Operations. *Annals of the CIRP* 56(1):365-368.

[5] Sencer B, Altintas Y, Croft E (2008) Feed Optimization for Five-Axis CNC Machine Tools with Drive Constraints. *Intl. J. Machine Tools & Manufacture* 48:733–745.

[6] Piazzi A., Visioli A., 1998, "Global Minimum-Time Trajectory Planning of Mechanical Manipulators Using Interval Analysis", *International Journal of Control,* Vol. 71, No. 4, pp. 631-652.

[7] Heng, M., 2008. M.A.Sc. Thesis: Smooth and Time-Optimal Trajectory Generation for High Speed Machine Tools. The University of Waterloo, Waterloo, Ontario.

[8] Altintas, Y., 2000, *Manufacturing Automation: Metal Cutting Mechanics, Machine Tool Vibrations, and CNC Design,* Cambridge University Press.

[9] Koren, Y., Lo, C.C., Shpitalni, M., 1993, "CNC Interpolators: Algorithms and Analysis", ASME Production Engineering Division, Proceedings of the 1993 ASME Winter Annual Meeting, Vol. 64, pp. 83-92.

[10] Bedi, S., Quan, N., 1992, "Spline Interpolation Technique for NC Machines", Computers in Industry, Vol. 18, No. 3, pp. 307-313.

[11] Erkorkmaz, K., Altintas, Y., 2001, "High Speed CNC System Design: Part I - Jerk Limited Trajectory Generation and Quintic Spline Interpolation", International Journal of Machine Tools and Manufacture, Vol. 41, No. 9, pp. 1323-1345.

[12] Wang, F.-C., Yang, D.C.H., 1993, Nearly Arc-Length Parameterized Quintic-Spline Interpolation for Precision Machining, Computer-Aided Design, 25/5: 281-288.

[13] Wang, F.-C., Wright, P. K., Barsky, B. A., Yang, D. C. H., 1999, Approximately Arc-Length Parameterized G^3 Quintic Interpolatory Splines, ASME Journal of Mechanical Design, 121/3:430-439.

[14] Erkorkmaz, K., Altintas, Y., 2005, Quintic Spline Interpolation with Minimal Feed Fluctuation, ASME Journal of Manufacturing Science and Engineering, 127/2:339-349.

[15] Piegl, L., Tiller, W., 2003, *The NURBS book, 2nd Edition*; Springer-Verlag, Berlin.

[16] Lee, R.S., Liang, S.P., 2006, A strain energy minimization method for generating continuous NURBS-based motion curves in free-form surface machining, International Journal of Advanced Manufacturing Technology, 28/11-12:1136-1145.

[17] Farouki R. T., Shah S., 1996, "Real-Time CNC Interpolators for Pythagorean-Hodograph Curves," *Computer Aided Geometric Design*, Vol. 13, No. 7, pp. 583-600.

[18] Farouki R. T., Al-Kandari M., Sakkalis T., 2002, "Hermite Interpolation by Rotation-Invariant Spatial Pythagorean-Hodograph Curves," *Advanced in Computational Mathematics*, Vol. 17, pp. 369-383.

[19] Erkorkmaz, K., 2004, Ph.D. Thesis: Optimal Trajectory Generation and Precision Tracking Control for Multi-Axis Machines. The University of British Columbia, Vancouver.

[20] Koninckx B., Van Brussel H., 2002, "Real-Time NURBS Interpolator for Distributed Motion Control", *Annals of CIRP* , Bol. 51, No. 1, pp. 315-318.

[21] Lartigue C., Thiebaut F., Maekawa T., 2001, "CNC Tool Path in Terms of B-Spline Curves", *Computer Aided Design*, Vol. 33, No. 4, pp. 307-319.

[22] Koch, P. E., Wang, K., 1988, "Introduction of B-splines to Trajectory Planning for Robot Manipulators", Modeling, Identification and Control, Vol. 9, No. 2, pp. 69-80.

[23] Affouard, A., Duc, E., Lartigue, C., Langeron, J.-M, Bourdet, P., 2004, "Avoiding 5-Axis Singularities Using Tool Path Deformation", International Journal of Machine Tools and Manufacture, Vol. 44, No. 4, pp. 415-425.

[24] Fleisig, R. V., Spence, A. D., 2001, "Constant Feed and Reduced Angular Acceleration Interpolation Algorithm for Multi-Axis Machining", Computer Aided Design, Vol. 33, No. 1, pp. 1-15.

[25] Muller, M., Erdos, G., Xirouchakis, P., 2004, "High Accuracy Spline Interpolation for 5-Axis Machining", Computer Aided Design, Vol, 36, No. 13, pp. 1379-1393.

[26] Langeron, J. M., Duc, E., Lartigue, C., Bourdet, P., 2004, "A New Format for 5-Axis Toolpath Computation Using B-spline Curves", CAD Computer Aided Design, Vol. 26, No. 12, pp. 1219-1229.

[27] Lartigue, C., Duc, E., Affouard, A., 2003, "Tool Path Deformation In 5-Axis Flank Milling Using Envelope Surface", Vol. 35, No. 4, pp. 375-382.

[28] Lin, R. -S., 2000, "Real-Time Surface Interpolator for 3-D Parametric Surface Machining On 3-Axis Machine Tools", International Journal of Machine Tools and Manufacture, Vol. 40, No. 10, pp. 1513-1526.

[29] Shpitalni M., Koren Y., Lo C.-C., 1994, "Realtime Curve Interpolators," *Computer Aided Design,* Vol. 26, No. 11, pp. 832-838.

[30] Huang, J.-T., Yang, D.C.H., 1992, Precision Command Generation for Computer Controlled Machines, Precision Machining: Technology and Machine Development and Improvement, ASME-PED, 58:89-104.

[31] Otsuki, T., Kozai, H., Wakinotani, Y., Fanuc Ltd., Yamanashi, Japan, 1998, Free-Form Curve Interpolation Method and Apparatus, United States Patent 5,815,401.

[32] Cheng, C.W., Tsai, M.C., Maciejowski, J., 2006, Feedrate control for Non Uniform rational B-spline motion command generation, in Proc. Institution of Mechanical Engineers, Part B: Journal of Engineering Manufacture, 220/B11: 1855-1861.

[33] Lei, W.T., Sung, M.P., Lin, L.Y., Huang, J.J., 2007, Fast real-time NURBS path interpolation for CNC machine tools, International Journal of Machine Tools and Manufacture, 47/10:1530-1541.

[34] Koren, Y. Lin, R. S. 1994, "Real-Time Five Axis Interpolator for Machining Ruled Surfaces", Proceedings of the 1994 International Mechanical Engineering Congress and Exposition, ASME Dynamic System and Control Division, Vol. 55-2, pp. 951-959.

[35] Koren, Y., 1995, "Five Axis Surface Interpolators", Annals of CIRP, Vol. 44, No. 1, pp. 379-382.

[36] Chen Y.-C., Tlusty J., 1995, "Effect of Low-Friction Guideways and Lead-Screw Flexibility on Dynamics of High-Speed Machines", *Annals of CIRP*, Vol. 44/1/1995, pp. 353-356.

[37] Jeon J.-W., Park S.-H., Kim D.-I., Kim S., 1993, "An Efficient Trajectory Generation for Industrial Robots", *Proceedings of the 28th Annual Meeting of the IEEE Industry Applications Conference*, Vol. 3, pp. 2137-2143.

[38] Erkorkmaz, K., 1999, M.A.Sc. Thesis: High Speed Contouring Control For Machine Tool Drives. The University of British Columbia, Vancouver.

[39] Macfarlane, S., Croft, E.A., 2001, Design of Jerk Bounded Trajectories for On-Line Industrial Robot Applications, Proceedings IEEE International Conference on Robotics and Automation, 1:979-984.

[40] Pritschow, G., 1997, Course notes: Steuerungtechnik der Werkzeugmaschinen und Industrieroboter (control techniques of machine tools and industrial robots), Institute of Control Technology for Machine Tools and Manufacturing Units, Stuttgart University, Germany.

[41] Makino H., Ohde T., 1991, "Motion Control of the Direct Drive Actuator", *Annals of CIRP*, Vol. 40/1/1991, pp.375-378.

[42] Tomita Y., Makino K., Sugimine M., Taniguchi N., 1996, "High-Response X-Y Stage System Driven by In-Parallel Linear Motors", *Annals of CIRP*, Vol. 45/1/1996, pp. 359-362.

[43] Visioli, A., 2000, "Trajectory Planning of Robot Manipulators By Using Algebraic and Trigonometric Splines", Robotica, Vol. 18, No. 6, pp. 611-631.

[44] Wang F.-C., Yang D. C. H., 1993, "Computation and Implementation of Digital Time-Optimal Feedback Controllers for an Industrial X-Y Robot Subjected to Path,

Torque, and Velocity Constraints", *International Journal of Robotics Research*, Vol. 12, No. 5, pp. 420-433.

[45] Butler J., Haack B., Tomizuka M., 1988, "Reference Generation for High Speed Coordinated Motion of a Two Axis System", *Symposium on Robotics, ASME Winter Annual Meeting, Chicago, Il, USA*, DSC Vol. 11, pp. 457-470.

[46] Sencer, B., 2005, M.A.Sc. Thesis: Five-Axis Trajectory Generation Methods. The University of British Columbia, Vancouver.

[47] Lin, M.-T., Tsai, M.-S., Yau, H.-T., 2007, Development of a dynamics-based NURBS interpolator with real-time look-ahead algorithm, International Journal of Machine Tool and Manufacture, 47/15:2246-2262.

[48] Liu, X., Ahmad, F., Yamazaki, K., Mori, M., 2005, Adaptive interpolation scheme for NURBS curves with the integration of machining dynamics, International Journal of Machine Tools and Manufacture, 45/4-5:433-444.

[49] Xu, R.Z., Xie, L., Li, C.X., Du., D.S., 2008, Adaptive parametric interpolation scheme with limited acceleration and jerk values for NC machining, International Journal of Advanced Manufacturing Technology, 36/3-4:343-354.

[50] Van Willigenburg L. G., 1993, "Computation and Implementation of Digital Time-Optimal Feedback Controllers for and Industrial X-Y Robot Subjected to Path, Torque, and Velocity Constraints", *International Journal of Robotics Research*, Vol. 12, No. 5, pp. 420-433.

[51] Constantinescu D., Croft E. A., 2000, "Smooth and Time-Optimal Trajectory Planning for Industrial Manipulators Along Specified Paths", *Journal of Robotic Systems*, Vol. 17, No. 5, pp. 233-249.

[52] Weck M., Meylahn A., Hardebusch C., 1999, "Innovative Algorithms for Spline-Based CNC Controller", *Production Engineering Research and Development in Germany; Annals of the German Academic Society for Production Engineering*, Vol. 6, No. 1, pp. 83-86.

[53] Dong, J., Ferreira, P.M., Stori, J.A., 2007, Feed-rate optimization with jerk constraints for generating minimum time trajectories, International Journal of Machine Tools and Manufacture, 47:1941-1955.

[54] Erdim, H., Lazoglu, I., Ozturk, B., 2006, Feedrate scheduling strategies for free-form surfaces, International Journal of Machine Tools and Manufacture, 46/7-8:747-757.

[55] Nocedal J, Wright SJ, Numerical Optimization, Springer, NY, 1999.

[56] Simon D., Isik C., 1991, "Optimal Trigonometric Robot Joint Trajectories", *Robotica,* Vol. 9, No. 4, pp. 379-386.

[57] Kyriakopoulos K. J., Saridis G. N., 1988, "Minimum Jerk Path Generation", *Proceedings of the IEEE Intl. Conf. on Robotics and Automation, Philadelphia, PA, USA,* pp. 364-369.

[58] Kyriakopoulos K. J., Saridis G. N., 1994, "Minimum Jerk for Trajectory Planning and Control", *Robotica,* Vol. 12, No. 2, pp. 109-113.

[59] Simon D., Isik C., 1993, "Suboptimal Robot Joint Interpolation within User-Specified Knot Tolerances", *Journal of Robotic Systems,* Vol. 10, No. 7, pp. 889-911.

[60] Piazzi A., Visioli A., 2000, "Global Minimum-Jerk Trajectory Planning of Robot Manipulators", *IEEE Transactions on Industrial Electronics,* Vol. 47, No. 1, pp. 140-149.

[61] Flash T., Hogan N., 1985, "The Coordination of Arm Movements: an Experimentally Confirmed Mathematical Model", *Journal of Neuroscience,* Vol. 5, pp. 1688-1703.

[62] Yeo C.Y., Tam S.C., Jana S., Lau M.W.S., 1994, “A Technical Review of the Laser Drilling of Aerospace Materials”, Journal of Materials Processing Technology, Vol. 42, pp. 15-49.

[63] Hu W., Shin Y.C., King G.B., 2010, “Micromachining of Metals, Alloys, and Ceramics by Picosecond Laser Ablation”, ASME Journal of Manufacturing Science and Engineering, Vol. 132/ 011009.

[64] Elfizy A., Method for Drilling Holes According to an Optimized Sequence, US Patent Application Pub. No US 2009/019669A1, Aug 6, 2009.

[65] Chakraborty N., Akella S., Wen J., 2007, “Coverage of a Planar Point Set with Multiple Constrained Robots”, Prof. *3*rd Annual IEEE Conf. Autom. Sci., Eng., Scottsdale, AZ, USA, Sept 22-25.

[66] Xidias E.K., Zacharia P.T., Aspragathos N.A., 2010, “Time-Optimal Task Scheduling for Articulated Manipulators”, Robotica, Vol. 28, pp. 427–440.

[67] Dinauer W.R., Weigman T.V., 2008, “Controller for a Laser Using Predictive Models for Materials Processing”, U.S. Patent 7,324,867 B2.

[68] Bohez, E. L. J., 2002, "Five-Axis Milling Machine Tool Kinematic Chain Design and Analysis", International Journal of Machine Tools and Manufacture, Vol. 42, No. 4, pp. 505-520.

[69] Ruegg, A., Gygax, P., 1992, "Generalized Kinematics Model for Three to Five-Axis Milling Mahcines and their Implementation in a CNC", Annals of CIRP, Vol. 41, No. 1, pp. 547-550.

[70] Yoshikawa, T., Foundations of Robotics, MIT Press, Cambridge, MA: 1990.

[71] Alzaydi A.A., Erkorkmaz K., Elfizy A., Engin S., 2010, “Time-Optimal Trajectory Generation for Laser Drilling”, Proc. 25th ASPE Annual Mtg., Atlanta, GA, Oct 31-Nov 5.

[72] Erkorkmaz K., Alzaydi A.A., Elfizy A., Engin S., 2011, “Time-Optimal Trajectory Generation for 5-Axis On-the-Fly Laser Drilling”, Annals of CIRP, 60/1 (*in-press*).

[73] S. Skogestad, I. Postlethwaite. "Multivariable Feedback Control: Analysis and Design, *2*nd Edition," Wiley, Nov 2005.